Supporting Information

Tuning Acceptor Properties via O/S Heteroatom Bridging in Extended-Conjugation Central Cores toward Efficient Organic Solar Cells

Jingyi Huo[a], Jie Wang[a], Jiong Yang[a], Zhaochen Suo[a], Jian Liu[a], Wendi Shi[a], Zhaoyang Yao[a], Chenxi Li[a], Xiangjian Wan*[a] and Yongsheng Chen[a]

[a] *State Key Laboratory of Elemento-Organic Chemistry, Frontiers Science Center for New Organic Matter, Key Laboratory of Functional Polymer Materials, Tianjin Key Laboratory of functional polymer materials, Academy for Advanced Interdisciplinary Studies, Nankai University, Tianjin, 300071, China.*

E-mail: xjwan@nankai.edu.cn.

1. General Experimental

All reactions and manipulations which are sensitive to moisture or air were performed under inert atmosphere of argon. All chemicals were purchased from *J&K*, Acros, Alfa and Aldrich, and were used as received. Petroleum ether refers to the fraction boiling in the 60–90 °C range. Anhydrous DCM, DCE, toluene and DMSO were freshly distilled from calcium hydride. TLC were performed on silica gel Huanghai HSGF254 plates and visualization of the developed chromatogram was performed by fluorescence quenching (λ_{max} = 254 nm). Flash chromatography was performed using silica gel (200−300 mesh) purchased from Qingdao Haiyang Chemical Co., China. NMR spectroscopy was recorded on a Bruker AV 400 spectrometer at 400 MHz (^{1}H NMR) and 101 MHz (^{13}C NMR). Chemical shifts were reported in ppm relative to internal TMS for ^{1}H NMR data, deuterated solvent for ^{13}C NMR data ($CDCl_3$, δ = 77.0). Data are presented in the following space: chemical shift, multiplicity, coupling constant in hertz (Hz), and signal area integration in natural numbers. High resolution mass spectrum (HRMS) was recorded on APEXII and ZAB-HS spectrometer using an electrospray ionization (ESI-TOF) source or a MatriX assisted laser desorption ionization (MALDI−TOF) source.

2. Materials and Synthesis

All reactions and manipulations were carried out under argon atmosphere with the use of standard Schlenk techniques. All starting materials were purchased from commercial suppliers and used without further purification unless indicated otherwise. Polymer donor PM6 (M_w around 40-50 kDa, polydispersity index of 2.3) and starting **material 1** were purchased from Solarmer Energy, Inc.

Synthetic Section and Supporting Schemes

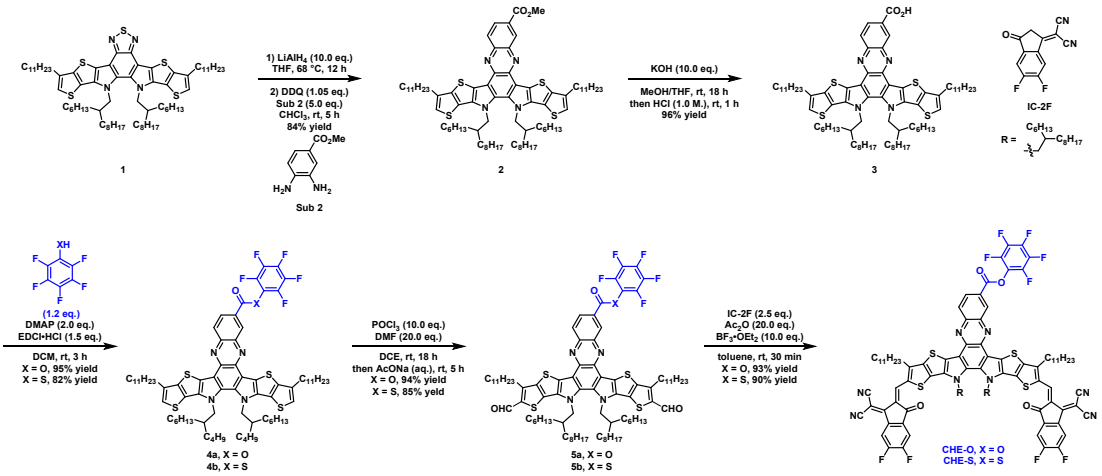

Scheme S1. The overall synthetic route to **CHE-O** and **CHE-S**.

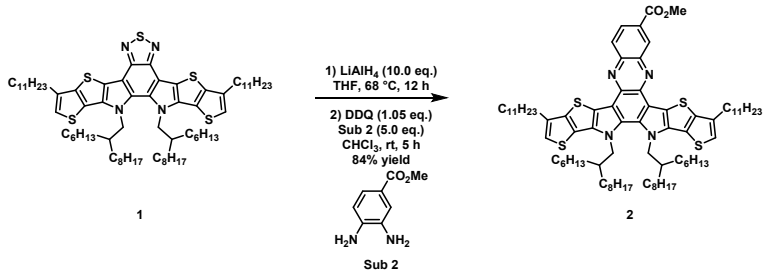

Scheme S2. Synthesis of **intermediate 2**.

Under the protection of nitrogen, compound 1 (598 mg, 0.5 mmol, 1.0 eq.) was dissolved in anhydrous tetrahydrofuran (THF, 30.0 mL). After that, a solution of Lithium aluminum hydride ($LiAlH_4$, 1.0 M, 5.0 mL, 10.0 eq.) was slowly added to the mixed solution. The resulting mixture was stirred and heated overnight, then the mixture was gently added to the saturated ammonium chloride (NH_4Cl) solution on ice and extracted with dichloromethane (DCM, 50.0 mL×3). The organic phase was dried over anhydrous sodium sulfate (Na_2SO_4) and concentrated under reduced pressure. The crude product was dissolved in a chloroform ($CHCl_3$, 50.0 mL) without further

purification. Then, 3-dichloro-5,6-dicyano-1,4-benzoquinone (DDQ, 125 mg, 0.55 mmol, 1.1 eq.) and methyl 3,4-diaminobenzoate (415 mg, 2.5 mmol, 5.0 eq.) are sequentially added to the solution. Stir the reactant at room temperature for 5 hours and remove the solvent under vacuum. The crude product was purified via silica gel column chromatography with hexane/dichloromethane (2:1, v/v) as eluent to afford intermediate 2 as a green solid (546 mg, 84% yield).

^{1}H NMR (400 MHz, $CDCl_3$) δ = 9.21 (s, 1H), 8.50 (d, *J* = 8.9 Hz, 1H), 8.42 (d, *J* = 8.9 Hz, 1H), 7.05 (s, 2H), 4.68 (d, *J* = 7.9 Hz, 4H), 4.10 (s, 3H), 2.90 (q, *J* = 7.4, 5.6 Hz, 4H), 2.18 (s, 2H), 1.93 (t, *J* = 8.0 Hz, 4H), 1.53–1.40 (m, 10H), 1.39–1.24 (m, 30H), 0.97 (ddd, *J* = 32.3, 13.4, 6.7 Hz, 41H), 0.80 (t, *J* = 7.3 Hz, 12H), 0.68 (t, *J* = 7.0 Hz, 6H).

^{13}C NMR (101 MHz, $CDCl_3$) δ = 167.07, 143.22, 140.26, 139.43, 139.15, 136.94, 132.49, 132.23, 131.55, 129.53, 129.11, 127.33, 123.60, 123.57, 123.45, 119.06, 117.03, 116.83, 55.13, 52.43, 38.73, 31.94, 31.77, 31.60, 30.50, 30.42, 29.92, 29.72, 29.68, 29.61, 29.57, 29.52, 29.50, 29.41, 29.38, 29.34, 29.12, 28.96, 28.94, 25.53, 22.70, 22.57, 22.45, 14.13, 14.07, 13.94.

HRMS (m/z) $[M]^+$ calcd. for ($C_{80}H_{120}N_4O_2S_4$): 1296.8294. Found: 1296.8356.

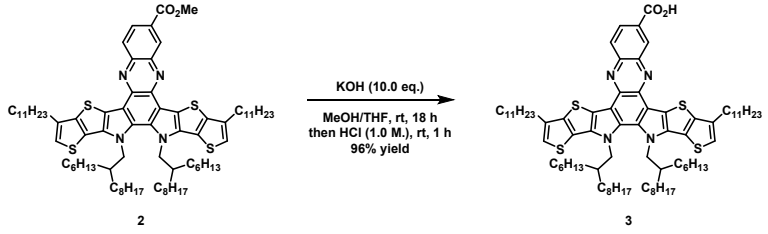

Scheme S3. Synthesis of **intermediate 3**.

Intermediate 2 (649 mg, 0.5 mmol, 1.0 eq.) was dissolved in tetrahydrofuran (30.0 mL), then 10.0 mL of a methanol (MeOH) solution containing 1.0 M KOH was slowly added to the reaction system. After the addition was completed, the reaction system was stirred at room temperature for approximately 12 h. Subsequently, 20 mL of 1.0 M hydrochloric acid (HCl, aq.) was dropwise to the reaction system to quench the reaction. The reaction system was extracted with dichloromethane (DCM, 50 mL×3), then the organic phase was separated and concentrated under reduced pressure. Finally, the crude product was purified via silica gel column chromatography with

dichloromethane/acetone (10:1, v/v) as eluent to afford intermediate 2 as a green solid (616 mg, 96%).

^{1}H NMR (400 MHz, $CDCl_3$) δ = 9.26 (s, 1H), 8.48 (d, *J* = 8.8 Hz, 1H), 8.41 (d, *J* = 8.9 Hz, 1H), 6.94 (d, *J* = 16.1 Hz, 2H), 4.59 (d, *J* = 7.7 Hz, 4H), 2.81 (d, *J* = 9.0 Hz, 4H), 2.10 (s, 2H), 1.84 (p, *J* = 7.4 Hz, 4H), 1.39 (dt, *J* = 23.7, 7.2 Hz, 10H), 1.22 (dd, *J* = 17.7, 12.1 Hz, 31H), 1.05 (p, *J* = 7.1 Hz, 10H), 0.94–0.83 (m, 30H), 0.71 (t, *J* = 7.2 Hz, 12H), 0.59 (t, *J* = 6.9 Hz, 6H).

^{13}C NMR (101 MHz, $CDCl_3$) δ = 170.84, 133.62, 128.09, 123.68, 55.15, 38.73, 31.95, 31.79, 31.62, 30.50, 30.42, 29.74, 29.71, 29.69, 29.62, 29.58, 29.54, 29.52, 29.43, 29.39, 29.36, 29.14, 28.97, 25.54, 22.72, 22.58, 22.47, 14.15, 14.09, 13.96.

HRMS (m/z) $[M]^+$ calcd. for ($C_{79}H_{118}N_4O_2S_4$): 1282.8138. Found:1282.8216.

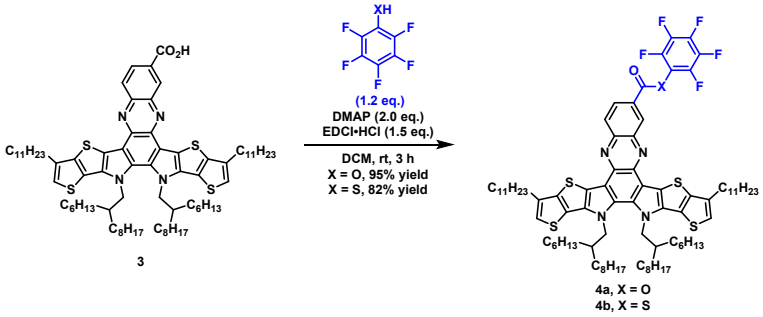

Scheme S4. Synthesis of **intermediate 4a-b**.

Synthesis of intermediate 4a：

Under the protection of nitrogen, Intermediate 3 (257 mg, 0.2 mmol, 1.0 eq.), 4-Dimethylaminopyridine (DMAP, 50 mg, 0.4 mmol, 2.0 eq.), *n*-(3-dimethylaminopropyl)-*n*'-ethyl carbodiimide hydrochloride (EDCI, 58 mg, 0.3 mmol, 1.5 eq.) and 2,3,4,5,6-pentafluoropheno (45 mg, 0.24 mmol, 1.2 eq.) dissolved in anhydrous dichloromethane (DCM, 20.0 mL) and stirred at room temperature for 12 h. Then, the reaction mixture is quenched by dropwise with saturated ammonium chloride solution (NH_4Cl, aq.) and extracted with dichloromethane (DCM, 50 mL×3). The combined organic phase was washed with saturated saline solution for three times and dried over anhydrous with sodium sulfate (Na_2SO_4). After solvent was evaporated under reduced pressure, the residue was purified through a silica gel column with petroleum ether/dichloromethane (1:1, v/v) as eluent to give compound 4a as a green

solid (276 mg, 95% yield).

^{1}H NMR (400 MHz, $CDCl_3$) δ = 9.39 (d, *J* = 1.9 Hz, 1H), 8.54 (d, *J* = 8.9 Hz, 1H), 8.45 (dd, *J* = 8.8, 2.0 Hz, 1H), 7.02 (s, 2H), 4.68–4.62 (m, 4H), 2.88–2.82 (m, 4H), 2.15 (q, *J* = 6.3 Hz, 2H), 1.91–1.84 (m, 4H), 1.49–1.43 (m, 4H), 1.39 (q, *J* = 6.5 Hz, 4H), 1.34 – 1.21 (m, 28H), 1.09 (dq, *J* = 10.0, 5.3, 3.6 Hz, 10H), 0.99–0.85 (m, 37H), 0.76 (t, *J* = 7.3 Hz, 9H), 0.64 (t, *J* = 7.0 Hz, 6H).

^{13}C NMR (101 MHz, $CDCl_3$) δ = 162.68, 143.86, 143.37, 143.30, 140.17, 139.93, 139.50, 137.20, 136.95, 134.44, 132.60, 131.70, 130.20, 127.26, 125.47, 123.70, 123.62, 123.44, 123.42, 119.29, 119.24, 116.94, 116.71, 55.21, 38.77, 38.74, 31.95, 31.91, 31.78, 31.60, 30.55, 30.51, 30.43, 29.73, 29.69, 29.65, 29.57, 29.50, 29.41, 29.35, 29.13, 28.94, 25.55, 22.71, 22.58, 22.45, 14.13, 14.10, 14.06, 13.94.

HRMS (m/z) $[M]^+$ calcd. for ($C_{85}H_{117}F_5N_4O_2S_4$): 1448.7980 Found:1448.8029.

Synthesis of intermediate 4b：

Intermediate 4b was obtained by a similar method with a yield of 82% yield and is a green solid.

^{1}H NMR (400 MHz, $CDCl_3$) δ = 9.27 (s, 1H), 8.55 (d, J = 8.9 Hz, 1H), 8.35–8.28 (m, 1H), 7.07 (d, J = 2.7 Hz, 2H), 4.70 (d, J = 7.8 Hz, 4H), 2.91 (td, J = 7.8, 4.2 Hz, 4H), 2.20 (s, 2H), 1.94 (q, J = 6.4 Hz, 4H), 1.51 (t, J = 7.6 Hz, 4H), 1.44 (t, J = 7.2 Hz, 4H), 1.39–1.21 (m, 30H), 1.16–1.12 (m, 6H), 1.06–0.87 (m, 40H), 0.81 (t, J = 7.2 Hz, 8H), 0.69 (t, J = 7.0 Hz, 6H).

^{13}C NMR (101 MHz, $CDCl_3$) δ = 184.86, 148.11, 147.97, 146.18, 145.62, 145.48, 144.43, 144.27, 143.85, 143.40, 143.32, 141.97, 141.81, 140.02, 139.81, 139.56, 137.22, 137.06, 136.99, 136.94, 133.68, 132.56, 131.73, 131.52, 130.41, 124.96, 123.68, 123.62, 123.43, 119.31, 119.25, 116.91, 116.75, 115.66, 55.21, 38.78, 38.74, 31.94, 31.92, 31.78, 31.60, 30.54, 30.49, 30.44, 30.18, 29.72, 29.70, 29.67, 29.59, 29.56, 29.50, 29.41, 29.38, 29.34, 29.13, 28.94, 26.76, 25.55, 25.53, 22.70, 22.58, 22.45, 14.12, 14.07, 13.93.

HRMS (m/z) $[M]^+$ calcd. for ($C_{85}H_{117}F_5N_4OS_5$): 1464.7751 Found:1464.7749.

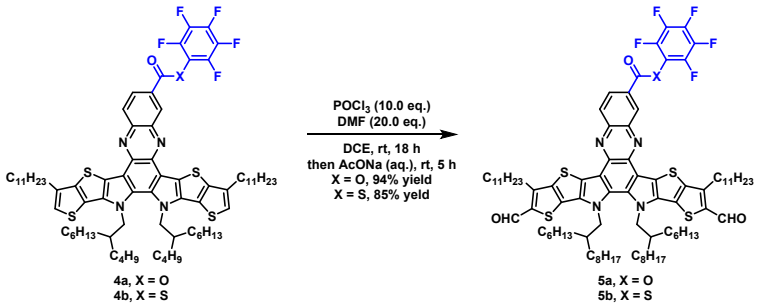

Scheme S5. Synthesis of **intermediate 5a-b**.

Synthesis of intermediate 5a：

Under the protection of nitrogen, phosphorus oxychloride ($POCl_3$, 0.5 mL) was added dropwise to a solution of anhydrous *N*,*N*-dimethylformamide (DMF, 1.0 mL) at 0°C and stirred at room temperature for 30 min. Intermediate 2 (200 mg, 0.15 mmol, 1.0 eq.) dissolved in anhydrous 1,2-dichloroethane (DCE, 20.0 mL) was add to the above solution and stirred at 85 °C for 12 h. Then, the reaction mixture is quenched by stirring with saturated sodium acetate (AcONa) solution and extracted with dichloromethane (DCM, 50 mL×3). The combined organic phase was washed with saturated saline solution (NaCl, aq.) for three times and dried over anhydrous with sodium sulfate (Na_2SO_4). After solvent was evaporated under reduced pressure, the residue was purified through a silica gel column with petroleum ether/dichloromethane (1:1, v/v) as eluent to give intermediate 5a as an orange red solid (213 mg, 94% yield).

^{1}H NMR (400 MHz, $CDCl_3$) δ = 10.19 (d, *J* = 2.2 Hz, 2H), 9.42 (d, *J* = 1.8 Hz, 1H), 8.60 (d, *J* = 8.9 Hz, 1H), 8.55 (dd, *J* = 8.8, 1.9 Hz, 1H), 4.72 (d, *J* = 7.9 Hz, 4H), 3.27 (q, *J* = 7.9, 7.3 Hz, 4H), 2.16 (q, *J* = 6.3 Hz, 2H), 2.00 (q, *J* = 7.0, 6.4 Hz, 4H), 1.55 (dt, *J* = 15.3, 7.2 Hz, 4H), 1.48–1.40 (m, 4H), 1.39–1.21 (m, 26H), 1.12 (dq, *J* = 14.5, 7.1 Hz, 12H), 1.06–0.93 (m, 30H), 0.88 (q, *J* = 6.8 Hz, 8H), 0.80 (t, *J* = 7.2 Hz, 8H), 0.69 (t, *J* = 6.9 Hz, 6H).

^{13}C NMR (101 MHz, $CDCl_3$) δ = 181.79, 162.43, 146.94, 146.92, 144.39, 144.33, 144.09, 140.32, 139.94, 139.43, 137.07, 137.04, 136.91, 136.78, 134.33, 133.67, 132.93, 130.28, 129.46, 128.40, 128.24, 128.01, 126.35, 117.70, 117.52, 55.44, 39.00, 38.97, 31.91, 31.88, 31.75, 31.59, 31.54, 30.56, 30.53, 30.49, 30.45, 30.39, 29.74,

29.71, 29.68, 29.64, 29.59, 29.56, 29.43, 29.39, 29.35, 29.29, 29.14, 28.22, 25.50, 22.69, 22.66, 22.56, 22.46, 14.12, 14.06, 13.94.

HRMS (m/z) $[M]^+$ calcd. for ($C_{87}H_{117}F_5N_4O_4S_4$): 1504.7878. Found:1504.7885.

Synthesis of intermediate 5b:

Intermediate 5b was obtained by a similar method with a yield of 82% yield and is a orange red solid.

^{1}H NMR (400 MHz, $CDCl_3$) δ = 10.10 (d, *J* = 1.7 Hz, 2H), 9.15 (d, *J* = 2.0 Hz, 1H), 8.48 (d, *J* = 8.9 Hz, 1H), 8.26 (dd, *J* = 8.9, 2.0 Hz, 1H), 4.65–4.58 (m, 4H), 3.19 (td, *J* = 7.9, 4.0 Hz, 4H), 2.06 (s, 2H), 1.91 (q, *J* = 6.9 Hz, 4H), 1.48–1.41 (m, 4H), 1.35 (d, *J* = 6.7 Hz, 4H), 1.26–1.15 (m, 30H), 1.04 (p, *J* = 6.8 Hz, 10H), 0.98–0.82 (m, 36H), 0.70 (t, *J* = 7.3 Hz, 8H), 0.59 (t, *J* = 6.9 Hz, 6H).

^{13}C NMR (101 MHz, $CDCl_3$) δ = 184.24, 181.80, 168.06, 167.76, 146.96, 146.91, 144.42, 144.34, 144.07, 140.41, 139.83, 139.50, 137.10, 137.05, 136.93, 136.81, 134.37, 133.64, 132.96, 132.45, 131.92, 131.37, 131.11, 130.88, 130.53, 129.48, 129.44, 128.88, 128.80, 128.37, 128.24, 125.74, 117.64, 117.52, 114.06, 68.16, 67.77, 55.45, 52.66, 39.00, 38.97, 38.91, 38.73, 38.54, 33.83, 33.22, 31.94, 31.91, 31.88, 31.75, 31.62, 31.54, 31.44, 30.56, 30.52, 30.47, 30.37, 30.19, 29.74, 29.71, 29.67, 29.63, 29.61, 29.56, 29.51, 29.44, 29.42, 29.38, 29.35, 29.32, 29.28, 29.16, 29.13, 28.99, 28.93, 28.22, 26.75, 25.91, 25.50, 23.99, 23.75, 22.99, 22.69, 22.66, 22.56, 22.45, 19.06, 14.12, 14.06, 13.98, 13.94, 13.66, 11.10, 10.97, 10.89.

HRMS (m/z) $[M]^+$ calcd. for ($C_{87}H_{117}F_5N_4O_4S_4$): 1504.7878. Found:1504.7885.

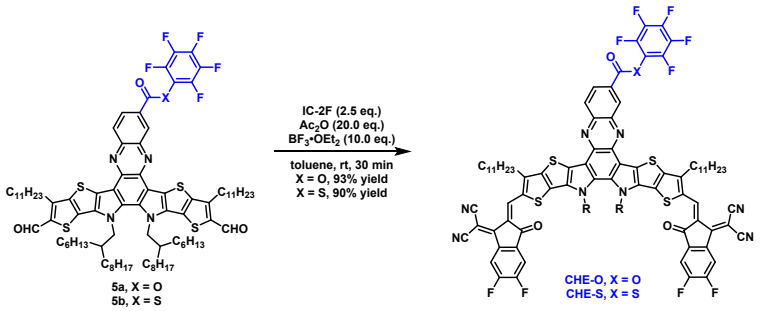

Scheme S6. Synthesis of **CHE-O** and **CHE-S**.

Synthesis of CHE-O:

Intermediate 5a (151 mg, 0.1 mmol, 1.0 eq.) and IC-2F (57 mg, 0.25 mmol, 2.5 eq.) were dissolved in toluene (20.0 mL), then 1.0 mL acetic anhydride (Ac_2O) and 0.2 ml

boron trifluoride diethyl etherate ($BF_3 \cdot OEt_2$) added separately. The resulting mixture was stirred 15 minutes at room temperature. Subsequently, 2.5 mL of methanol (MeOH) was added to the reaction system to quench the reaction. The reaction mixture concentrated under reduced pressure. The crude product was purified via silica gel column chromatography with petroleum ether/chloroform (1:1, v/v) as eluent to afford CHE-O as a black solid (176 mg, 93%).

^{1}H NMR (400 MHz, $CDCl_3$) δ = 10.19 (d, *J* = 2.2 Hz, 2H), 9.42 (d, *J* = 1.8 Hz, 1H), 8.60 (d, *J* = 8.9 Hz, 1H), 8.55 (dd, *J* = 8.8, 1.9 Hz, 1H), 4.72 (d, *J* = 7.9 Hz, 4H), 3.27 (q, *J* = 7.9, 7.3 Hz, 4H), 2.16 (q, *J* = 6.3 Hz, 2H), 2.00 (q, *J* = 7.0, 6.4 Hz, 4H), 1.55 (dt, *J* = 15.3, 7.2 Hz, 4H), 1.48–1.40 (m, 4H), 1.39–1.21 (m, 26H), 1.12 (dq, *J* = 14.5, 7.1 Hz, 12H), 1.06–0.93 (m, 30H), 0.88 (q, *J* = 6.8 Hz, 8H), 0.80 (t, *J* = 7.2 Hz, 8H), 0.69 (t, *J* = 6.9 Hz, 6H).

^{13}C NMR (101 MHz, $CDCl_3$) δ = 181.79, 162.43, 146.94, 146.92, 144.39, 144.33, 144.09, 140.32, 139.94, 139.43, 137.07, 137.04, 136.91, 136.78, 134.33, 133.67, 132.93, 130.28, 129.46, 128.40, 128.24, 128.01, 126.35, 117.70, 117.52, 55.44, 39.00, 38.97, 31.91, 31.88, 31.75, 31.59, 31.54, 30.56, 30.53, 30.49, 30.45, 30.39, 29.74, 29.71, 29.68, 29.64, 29.59, 29.56, 29.43, 29.39, 29.35, 29.29, 29.14, 28.22, 25.50, 22.69, 22.66, 22.56, 22.46, 14.12, 14.06, 13.94.

HRMS (m/z) $[M]^+$ calcd. for ($C_{111}H_{121}F_9N_8O_4S_4$): 1929.8283. Found:1929.8305.

Synthesis of CHE-S：

CHE-S was obtained by a similar method with a yield of 90% yield and is a black solid.

^{1}H NMR (400 MHz, $CDCl_3$) δ = 9.18 (d, *J* = 4.8 Hz, 3H), 8.57 (dd, *J* = 9.9, 6.4 Hz, 2H), 8.52 (d, *J* = 8.9 Hz, 1H), 8.34 (dt, *J* = 8.8, 2.9 Hz, 1H), 7.72 (t, *J* = 7.5 Hz, 2H), 4.83 (d, *J* = 8.0 Hz, 4H), 3.29 (s, 4H), 2.23 (s, 2H), 1.91 (s, 4H), 1.55 (d, *J* = 12.3 Hz, 8H), 1.41 (s, 4H), 1.28 (d, *J* = 19.5 Hz, 30H), 1.00 (s, 36H), 0.84 (dt, *J* = 10.6, 6.4 Hz, 8H), 0.74 (t, *J* = 7.2 Hz, 6H), 0.67 (t, *J* = 6.7 Hz, 6H).

^{13}C NMR (101 MHz, $CDCl_3$) δ = 185.45, 153.31, 145.62, 137.05, 135.16, 134.65, 134.01, 133.44, 132.62, 131.24, 119.31, 118.09, 114.28, 113.88, 68.10, 55.24, 38.65, 31.26, 31.23, 31.17, 30.95, 30.80, 29.99, 29.23, 29.14, 29.04, 29.02, 28.99, 28.96,

28.89, 28.84, 28.71, 28.66, 28.53, 25.02, 22.02, 21.99, 21.92, 21.82, 13.44, 13.39, 13.33.

HRMS (m/z) $[M]^+$ calcd. for ($C_{111}H_{121}F_9N_8O_3S_5$): 1945.8055. Found:1945.7988.

Isotopic peaks observed：[M+2]: 1947.8086. [M+4]:1949.8065.

3. Device Fabrication and Characterization

3.1 Device fabrication

The conventional devices were fabricated with the architecture of ITO/ 2PACz/active layer/PNDIT-F3N/Ag. In detail, ITO coated glass substrates were cleaned in turn with detergent water, deionized water, acetone and isopropyl alcohol in an ultrasonic bath sequentially for 15 mins and dried by nitrogen purge. Before use, the cleaned ITO substrates were treated with UV exposure for 15 mins in a UV-ozone chamber (Jelight Company). Then a thin layer of 2PACz was first spin-coated on the ITO substrates with 3000 rpm for 20 s with thermal annealed for 5 minutes at 100 °C. The PM6: CHE-O (1:1.2 w/w) was dissolved in chloroform at the total blend concentration of 14.3 mg/mL with 70% TCB. The active layer was spin-coated at 2000 rpm for 30 s onto the hole transport layer. The PM6: CHE-S (1:1.2 w/w) were dissolved in chloroform at the total blend concentration of 13.2 mg/mL. All the solutions need to be stirred at room temperature overnight. Then the active layer was spin-coated at 2000 rpm for 30 s onto the hole transport layer. After spin coating, the blend films were annealed at 80 °C for 10 mins. PNDIT-F3N (dissolved in methanol with 0.5% v/v glacial acetic acid at the concentration of 1 mg mL^{-1}) layer was spin-coated on the top of the active layers at 3000 rpm for 20 s. Finally, 150 nm Ag was deposited under 2×10^{-6} Pa. The active area

of the device was 4 mm^2, respectively. The device and mask areas were determined using an optical profilometer (PSM-1000).

3.2 Characterization of the OSC

The J-V measurements were performed by using the solar simulator (SS-F5-3A, Enli Technology, xenon lamp, filter model AMFG2.0) along with AM 1.5G spectra (100 mW cm^{-2}), Which was calibrated by a standard Si solar cell (made by Enli Technology Co., Ltd., Taiwan, and calibrated report can be traced to NREL. The spectral between reference cell and devices could match well during the test (within 5% errors). The current-voltage scan speed and delay time are 0.02 V/s and 1 ms respectively. No pretreatments (light soaking or holding cell at a bias) were required before J-V testing, and all the measurements were conducted in a nitrogen-filled glovebox at room temperature (ca. 25°C) without attaching any antireflection coating on the incident plane of solar cells. Note that there are no hysteresis or other unusual behaviors during the measurements of solar cells. The EQE spectra were measured by using a QE-R Solar Cell Spectral Response Measurement System (Enli Technology Co., Ltd., Taiwan).

4. Measurements and Instruments

4.1 Supplementary Note 1

The ground-state (S_0) geometries and frontier molecular orbital energy levels of the studied molecules were optimized using density functional theory (DFT) with the Becke three-parameter Lee-Yang-Parr (B3LYP) hybrid functional [1]. Among them, the 6-31G(d) basis set was employed for light atoms (C, H, O, N, S, F) [2]. To reduce computational costs, all alkyl chains were replaced with methyl groups (-CH_3). Vibrational frequencies were calculated after geometry optimization, and no imaginary

frequencies were found. All calculations were performed using the Gaussian 16 package [3].

4.2 Supplementary Note 2.

UV-Visible (UV-vis) Absorption.

The UV-vis spectra were obtained by a Cary 5000 UV-vis spectrophotometer.

Cyclic Voltammetry (CV).

The CV experiments were performed with a LK98B II Microcomputer-based Electrochemical Analyzer. All measurements were conducted at room temperature with a three-electrode configuration. Among them, a glassy carbon electrode was employed as the working electrode, with a circular surface and a radius of 2.0 mm**,** a saturated calomel electrode (SCE) was used as the reference electrode, and a Pt wire was used as the counter electrode, and the solvent system was deoxygenated by bubbling with argon gas for 30 minutes. Tetrabutylammonium phosphorus hexafluoride ($n$$Bu_4NPF_6$, 0.1 M) in acetonitrile was employed as the supporting electrolyte, and the scan rate was kept at 100 mV s^{-1}, and the measurements were carried out at room temperature. After the measurements, the surface of the working electrode was cleaned and polished using Al_2O_3 as the polishing agent. Electrochemically reversible ferrocene was employed as internal reference. The HOMO and LUMO energy levels were calculated from the onset oxidation and the onset reduction potentials, respectively, by following the Supplementary **Equation S1–S2**:

$$E_{\mathrm{HOMO}} = -(4.80 + E_{ox}^{onest}) \text{ eV (S1)}$$

$$E_{\mathrm{LUMO}} = -(4.80 + E_{re}^{onest}) \text{ eV (S2)}$$

Photoluminescent (PL)

Steady-state photoluminescence measurements were performed using a FLS1000 spectrometer. The emission spectra of the four non-fullerene acceptors (NFAs) were recorded with a near-infrared (NIR) 5509 photomultiplier tube (PMT). For two NFAs (CHE-O and CHE-S), the excitation wavelength for their solutions was 650 nm, respectively, while the excitation wavelengths for their thin films were 762 nm.

Atomic Force Microscopy Based Infrared Spectroscopy (AFM-IR). The AFM-IR

images were performed using in tapping mode on a Bruker nano IR 3. AFM-IR images of the corresponding blend films measured at a wavenumber of 2216 cm^{-1}, which is a characteristic absorption peak of the C≡N bond in SMAs, compared with donor. All film samples were spin–cast on ITO/2PACz substrates under the same conditions as those used for device fabrication.

Grazing Incidence Wide Angle X-ray Scattering (GIWAXS).

The GIWAXS samples were prepared on Si substrates by use of the same preparation conditions with devices and were carried out at XEUSS SAXS/WAXS equipment.

The Energy Loss Analysis.

The following equation was used to quantify the E_{loss} of OSCs: $E_{\text{loss}} = E_g^{pv} - qV_{oc} = \left(E_g^{pv} - qV_{oc}^{SQ}\right) + \left(qV_{oc}^{SQ} - qV_{oc}^{rad}\right) + \left(qV_{oc}^{rad} - qV_{oc}\right) = \Delta E_1 + \Delta E_2 + \Delta E_3$. E_g^{pv} represents the bandgap of the blend film and q is the elementary charge. E_g^{pv} is estimated by the derivatives of the sensitive EQE spectra (dEQE/dE) for optimized OSCs.

The total E_{loss} can be divided into three parts:

(1) $\Delta E_1 = E_g - qV_{oc}^{SQ}$ represents the unavoidable radiative loss originating from absorption above the bandgap. The V_{oc}^{SQ} is the maximum voltage based on the Shockley–Queisser (SQ) limit (**Equation S3**):

$$V_{oc}^{SQ} = \frac{kT}{q}\ln\left(\frac{J_{sc}^{SQ}}{J_0^{SQ}} + 1\right) \cong \frac{kT}{q}\ln\left(\frac{q\bullet\int_{E_g}^{+\infty}\phi_{AM\,1.5G}\ (E)\ dE}{q\bullet\int_{E_g}^{+\infty}\phi_{BB}\ (E)\ dE}\right) \quad \text{(S3)}$$

(2) $\Delta E_2 = qV_{oc}^{SQ} - qV_{oc}^{rad}$ can be regarded as radiative loss caused by absorption below the bandgap, where the V_{oc}^{rad} is the open circuit voltage when there is only radiative recombination. The radiative recombination limit for the saturation current (J_{oc}^{rad}) is also calculated from the EQE spectrum (**Equation S4**):

$$V_{oc}^{rad} = \frac{kT}{q}\ln\left(\frac{J_{sc}}{J_0^{rad}}+1\right) \cong \frac{kT}{q}\ln\left(\frac{q\bullet\int_{E_g}^{+\infty} EQE(E)\phi_{AM\,1.5G}\ (E)\ dE}{q\bullet\int_{E_g}^{+\infty} EQE(E)\phi_{BB}\ (E)\ dE}\right) \quad \text{(S4)}$$

where q is the elementary charge and ϕ_{BB} is the black body spectrum at 300 K.

(3) $\Delta E_3 = qV_{oc}^{rad} - qV_{oc}$ (S5) can be directly calculated while the other two parts were determined.

Photoluminescence Quantum Yield (PLQY).

The PLQY was estimated by using an Edinburgh FLS1000 spectrometer which is equipped with an integrating sphere (HORIBA, Japan). The excitation wavelength and emission wavelength are 762 nm. The signal of four NFAs were recorded by an NIR photomultiplier (PMT-1700 nm) cooled to −80 ℃ with liquid N_2 and the wavelength detection range is between 800 nm and 1200 nm.

Electroluminescence External Quantum Efficiency (EQE_{EL}).

For the EQE_{EL} measurements, a digital source meter (Keithley 2400) was employed to inject electric current into the solar cells, and the emitted photons were collected by a Si diode 10 (Hamamatsu s1337-1010BQ) and indicated by a picometer (Keithley 6482). The injection current to the OSCs was kept at 1 mA by the direct current meter (PWS2326Tectronix). The Calculation of Non-Radiative Energy Loss: ΔE_3 is confirmed by directly measuring the external quantum efficiency of electroluminescence (EQE_{EL}) of the solar cell through the **Equation S6**:

$$\Delta E_3 = kTln(\frac{1}{EQE_{EL}}) \quad \text{(S6)}$$

5. Supporting Tables and Figures

5.1 Supporting Tables

Table S1. Photoelectric properties of two SMAs as solution and neat films.

Materials	λ_{sol}^{max} **[nm]**	λ_{film}^{max} **[nm]**	Δ_λ**[nm]** [a]	α_{max} **[M^{-1} cm^{-1}]**	λ_{onset} **[nm]**
CHE-O	739	804	65	1.89×10^5	905

CHE-S	739	800	61	1.73×10^5	905

[a]$\Delta\lambda = \lambda_{max}^{film} - \lambda_{max}^{sol}$.

Table S2. Summary of energy levels of two SMAs in neat film.

Materials	E_g^{opt} **[eV]** [a]	E_{Homo}^{cv} **[eV]**	E_{lumo}^{cv} **[eV]**	E_g^{cv} **[eV]**
CHE-O	1.37	-5.69	-3.87	1.82
CHE-S	1.37	-5.70	-3.87	1.83

[a] $E_g^{opt} = 1240/\lambda_{edg}^{film}$.

Table S3. Detailed parameters of corresponding two-dimensional grazing incidence wide-angle X-ray scattering (GIWAXS) for neat film of **CHE-O** and **CHE-S**.

Materials	**(010) Diffraction Peak**				**(100) Diffraction Peak**			
	q (Å^{-1})	d[a] (Å)	**FWHM** (Å^{-1})	**CCL**[b] (Å)	q (Å^{-1})	d[a] (Å)	**FWHM** (Å^{-1})	**CCL**[b] (Å)
CHE-O	1.730	3.63	0.203	27.84	0.348	18.05	0.169	33.44
CHE-S	1.704	3.69	0.264	21.41	0.315	19.94	0.176	32.11

[a] Calculated from the equation: d-spacing=2π/q. [b] Obtained from the Scherrer equation: CCL= 2πK/FWHM, where FWHM is the full-width at half-maximum and K is a shape factor (K= 0.9 here).

Table S4. The optimal photovoltaic parameters of **PM6: CHE-O**-based devices with different D:A ratios under AM 1.5G illumination (100 mW cm^{-2}).

D:A (w:w)	V_{oc} **(V)**	J_{sc} **(mA/cm^2)**	**FF (%)**	**PCE**
1:1.1	0.899	24.92	77.30	17.26
1:1.2	0.899	25.31	78.18	17.73

1:1.3	0.901	25.10	77.53	17.48

Table S5. Detailed photovoltaic parameters of the **PM6: CHE-O**-based devices processed by varied concentration of donor under the illumination of AM 1.5G Illumination (100 mW cm^{-2}).

Donor	V_{oc} **(V)**	J_{sc} **(mA cm^{-2})**	**FF(%)**	**PCE (%)**
6 mg/ml	0.902	26.41	79.79	19.00
6.5 mg/ml	0.895	26.68	80.11	19.14
7 mg/ml	0.900	26.08	79.97	18.78

Table S6. The optimal photovoltaic parameters of **PM6: CHE-O**-based devices with different ratio of TCB under AM 1.5G illumination (100 mW cm^{-2}).

Ratio(v/v)	V_{oc} **(V)**	J_{sc} **(mA cm^{-2})**	**FF(%)**	**PCE (%)**
60%	0.898	26.41	79.82	18.93
70%	0.895	26.91	80.15	19.30
80%	0.897	26.64	79.61	19.02

Table S7. Total energy loss values and different contributions in solar cells based on the SQ limit theory.

Active Layer	E_g	V_{oc}^{SQ} **(V)**	ΔE_1 **(eV)**	V_{oc}^{rad} **(V)**	ΔE_2 **(eV)**	ΔE_3**[a] (eV)**	ΔE_3**[b] (eV)**	V_{oc} **(V)**	E_{loss} **(eV)**
PM6: CHE-O	1.446	1.179	0.267	1.128	0.048	0.236	0.231	0.895	0.551
PM6: CHE-S	1.446	1.179	0.267	1.131	0.051	0.233	0.229	0.895	0.551

[a]$\Delta E_3 = q^{V_{oc}^{rad}} - qV_{oc}$; [b]$\Delta E_3 = -k\mathrm{Tln}\ (\mathrm{EQE_{EL}})$.

Table S8. Information about surface energies of **PM6**, **CHE-O** and **CHE-S** neat films calculated by water and glycerol contact angle.

Materials	θwater (°)	θglycerol (°)	γ_d (mN m^{-1})	γ_p (mN m^{-1})	γ (mN m^{-1})	$\chi_{D:A}$ [a] (K)
PM6	108.92	97.53	0.10	22.91	23.01	–
CHE-O	106.05	96.81	0.19	24.66	25.04	0.03
CHE-S	102.53	92.39	0.22	29.04	29.26	0.25

[a] The molecular miscibility can be evaluated by Flory–Huggins interaction parameter χ, which is calculated by using the equation of: $\chi_{D:A}=K(\sqrt{\gamma D}-\sqrt{\gamma A})^2$.

Table S9. Detailed parameters of corresponding two-dimensional GIWAXS for blend film of **PM6: CHE-O** and **PM6: CHE-S**.

Materials	**(010) Diffraction Peak**				**(100) Diffraction Peak**			
	q **(Å^{-1})**	***d*** **[a] (Å)**	**FWHM (Å^{-1})**	**CCL[b] (Å)**	***q*** **(Å^{-1})**	***d*** **[a] (Å)**	**FWHM (Å^{-1})**	**CCL[b] (Å)**
PM6: CHE-O	1.733	3.62	0.170	33.25	0.306	20.52	0.048	117.75
PM6: CHE-S	1.710	3.67	0.201	28.12	0.312	20.13	0.057	99.16

[a] Calculated from the equation: *d*-spacing=2π/q. [b] Obtained from the Scherrer equation: CCL= 2πK/FWHM, where FWHM is the full-width at half-maximum and K is a shape factor (K= 0.9 here).

Table S10. Statistical analysis of device parameters for eight independent devices based on **PM6: CHE-O** and **PM6: CHE-S**.

Device	V_{oc} [V]	J_{sc} [mA cm^{-2}]	FF [%]	PCE [%]
PM6: CHE-O	0.903	26.70	79.83	19.23
	0.898	27.03	79.37	19.26
	0.895	26.83	79.70	19.13
	0.899	26.83	79.62	19.21
	0.895	26.68	80.11	19.14
	0.900	26.49	80.48	19.19
	0.898	26.57	80.11	19.12
	0.895	26.91	80.15	19.30
Average value	0.898	26.76	79.92	19.20
PM6: CHE-S	0.894	25.12	73.53	16.52
	0.892	25.13	73.47	16.46
	0.891	24.87	73.38	16.26
	0.898	25.52	73.41	16.82
	0.895	25.83	73.13	16.89
	0.894	25.28	73.15	16.53
	0.893	25.29	73.31	16.56
	0.895	24.53	73.41	16.13
Average value	0.894	25.20	73.35	16.52

5.2 Supporting Figures

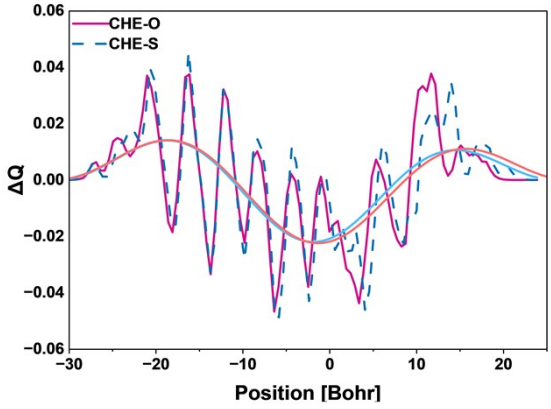

Figure S1: Theoretically calculated frontier orbital charge density differences (ΔQ).

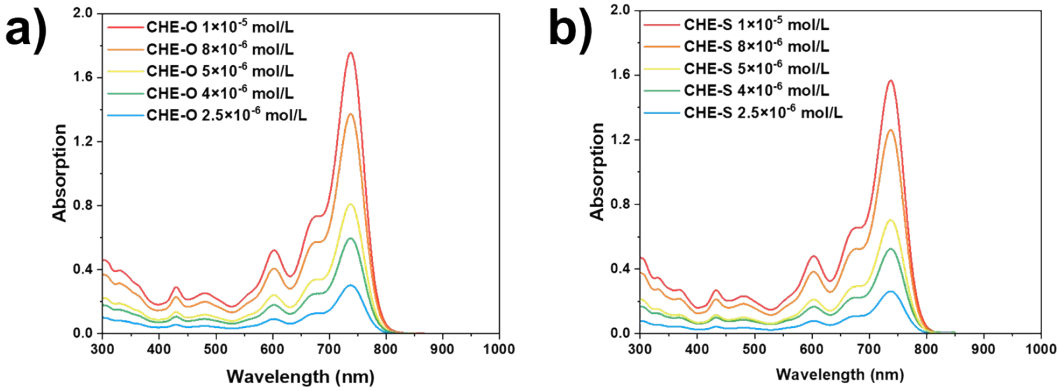

Figure S2: UV-Vis absorption spectra of CHE-O and CHE-S at different concentrations.

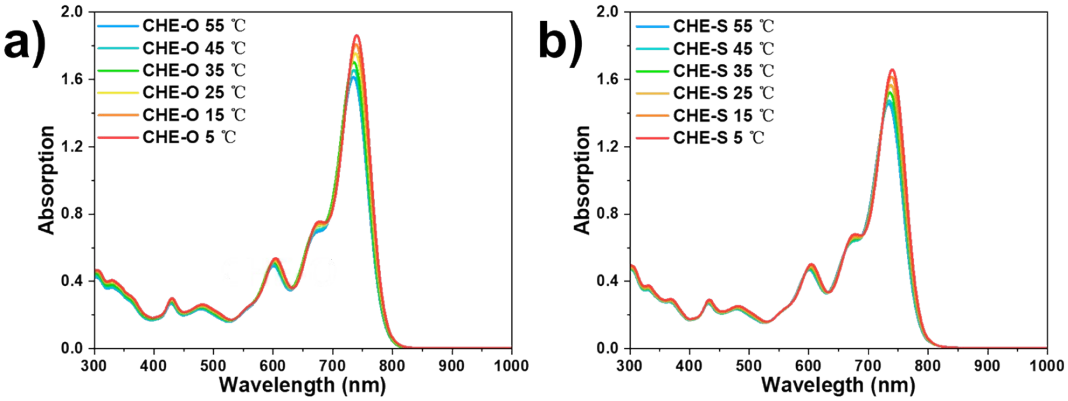

Figure S3: UV-Vis absorption spectra of CHE-O and CHE-S at a concentration of 1.0 × 10^{-5} mol/L over a temperature range of 5 °C to 55 °C.

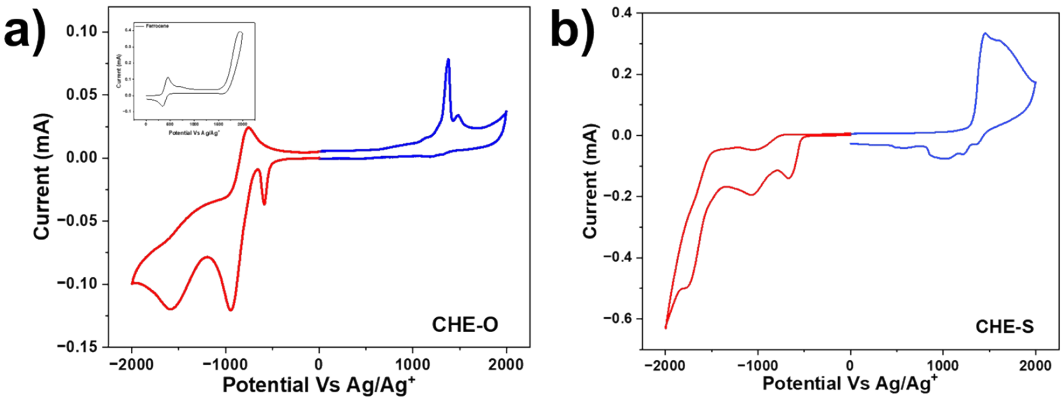

Figure S4: Cyclic voltammograms of CHE-O and CHE-S neat films. blue line: oxidation cycle, red line: reduction cycle.

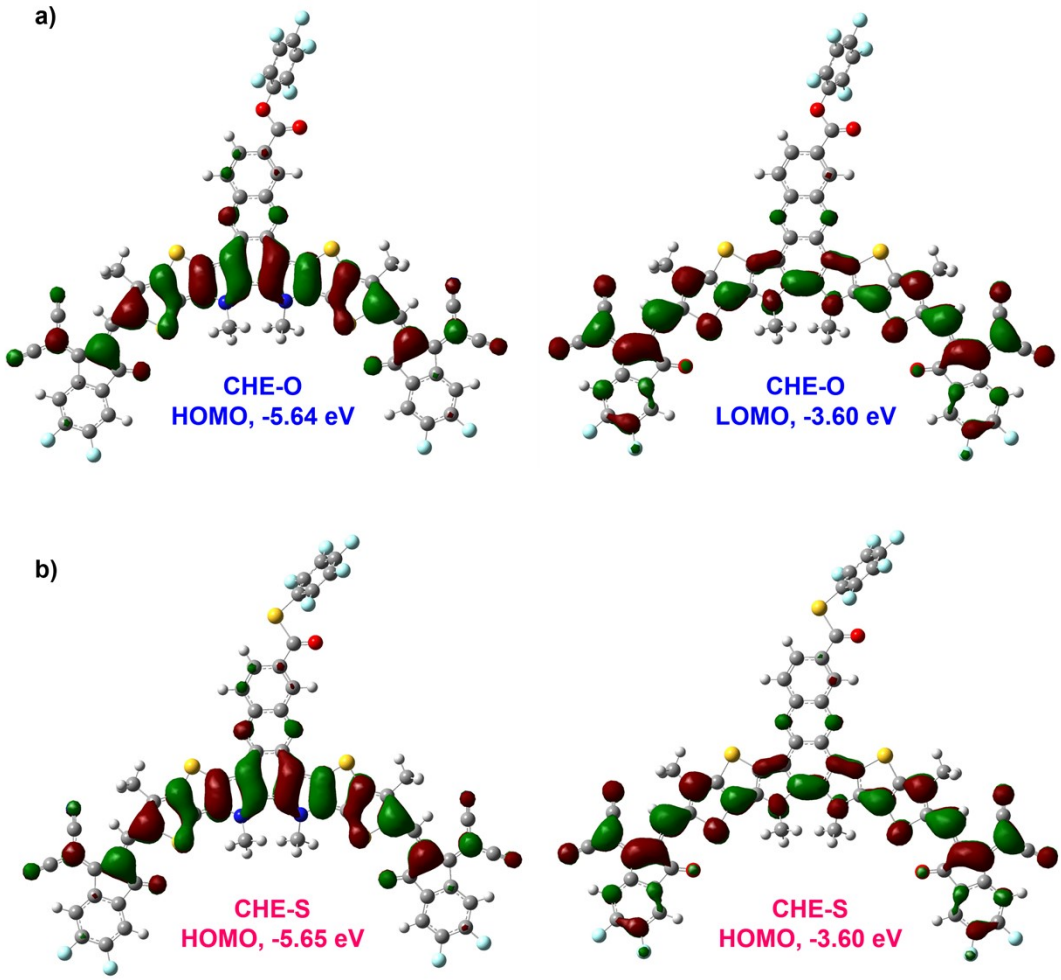

Figure S5: DFT theoretical density distribution for the frontier molecular orbits of CHE-O and CHE-S.

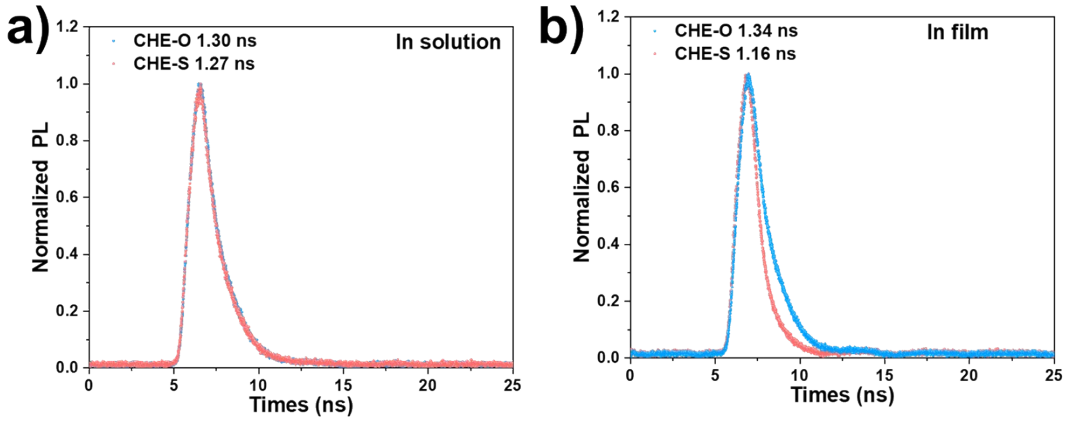

Figure S6: Time-resolved photoluminescence (PL) decay traces of CHE-O and CHE-S (a) in chloroform solutions and (b) neat films.

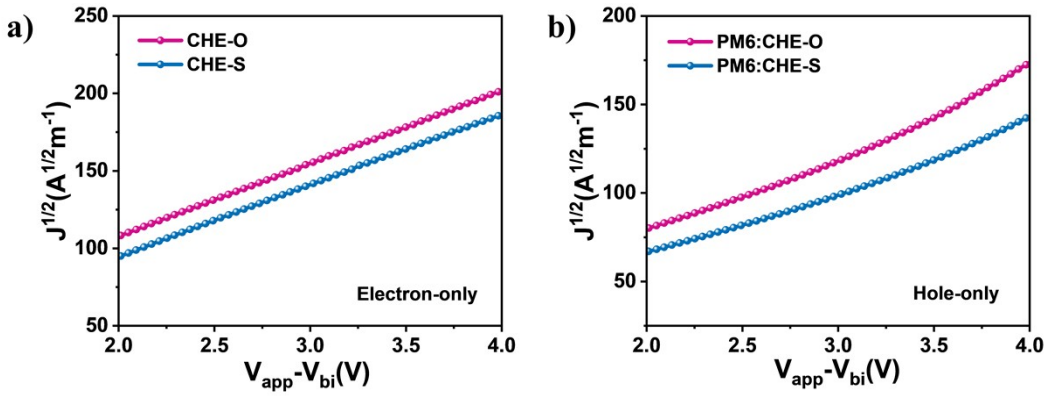

Figure S7: (a) Electron and (b) hole mobilities of PM6: CHE-O and PM6: CHE-S blended films.

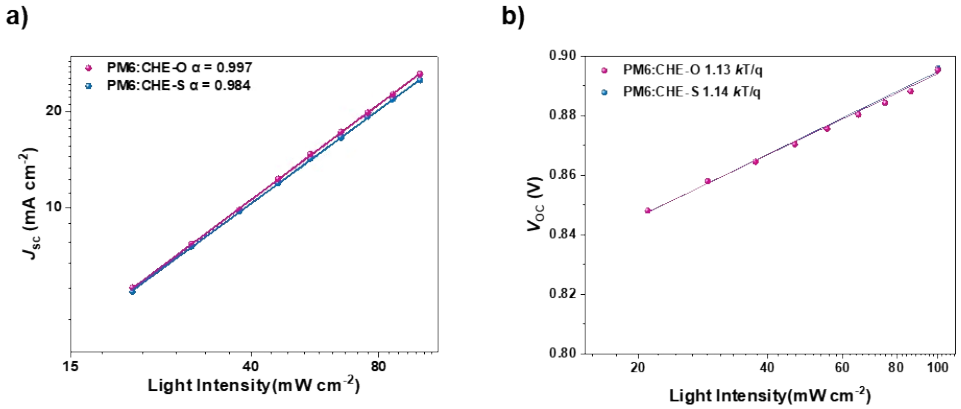

Figure S8: Light intensity (P_{light}) dependence of J_{sc} (a) and V_{OC} (b).

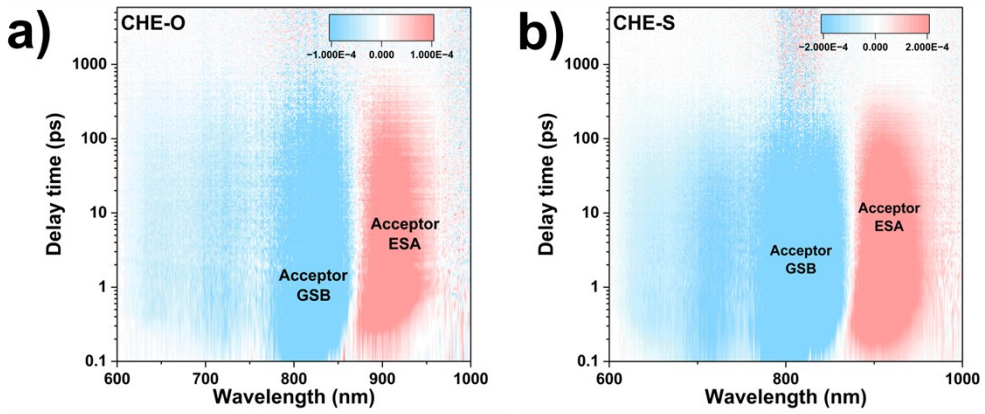

Figure S9: Color plots the fs-TA spectra of the CHE-O and CHE-S neat films.

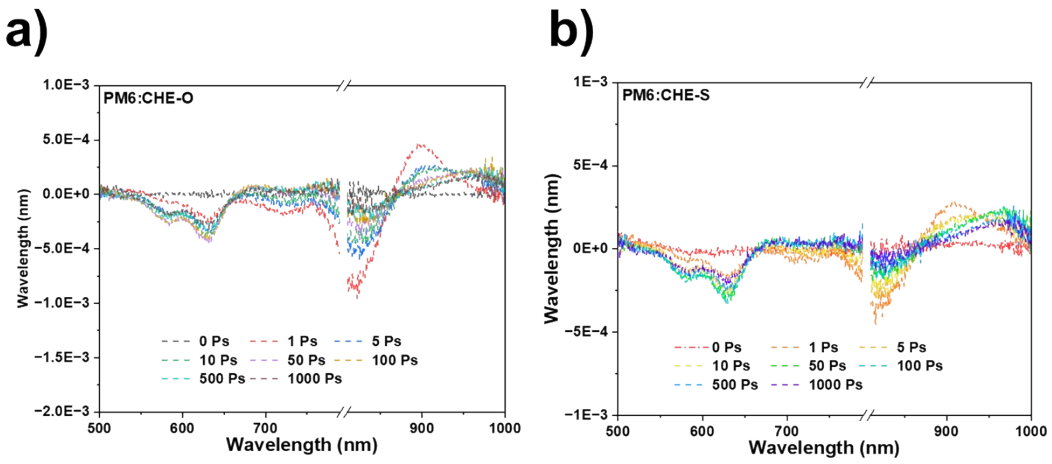

Figure S10: fs-TA spectra at different time delays of PM6: CHE-O and PM6: CHE-S blend films.

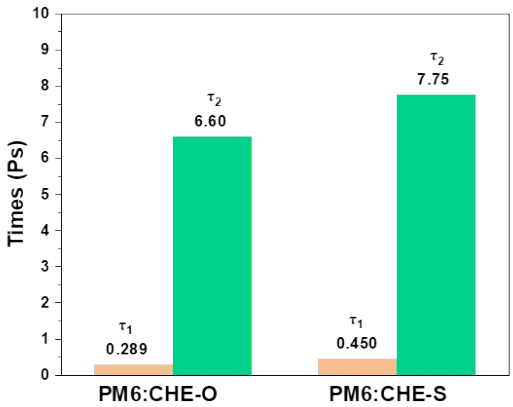

Figure S11: Exciton dynamics time achieved through a biexponential fitting for different blend films.

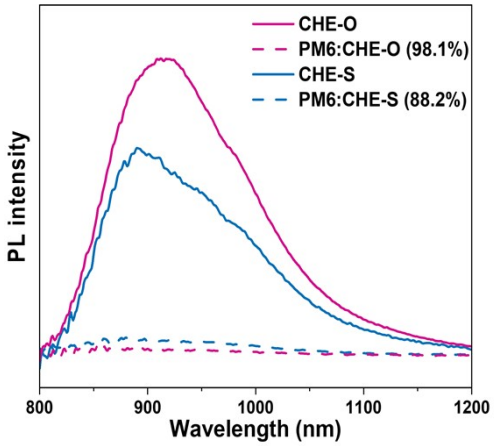

Figure S12: The photoluminescence (PL) quenching measurement of the CHE-O and CHE-S neat films and PM6: CHE-O and PM6: CHE-S blend films.

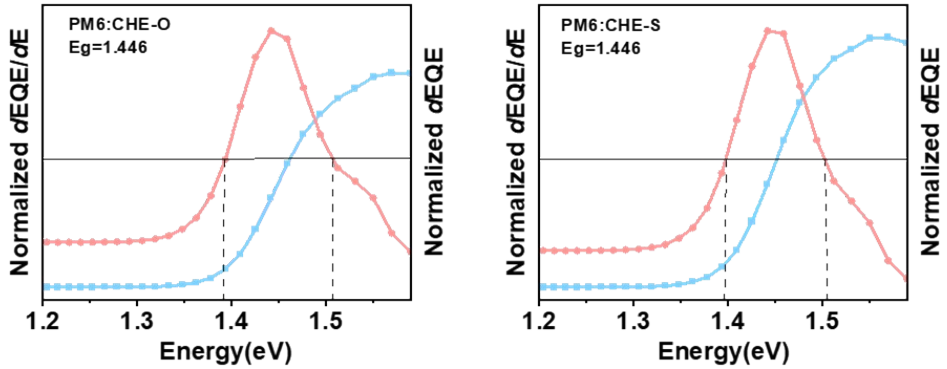

Figure S13: Optical bandgap determination of PM6: CHE-O and PM6: CHE-S blended films by the derivatives of the sensitive EQE spectra (*d*EQE/*d*E) for optimized OSCs.

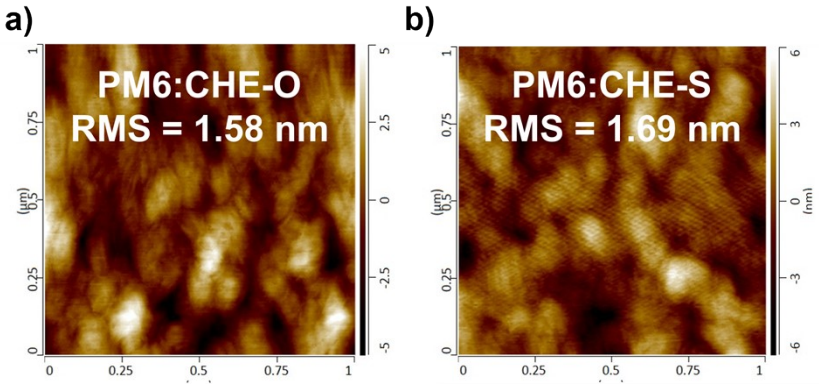

Figure S14: The AFM phase height of PM6: CHE-O and PM6: CHE-S.

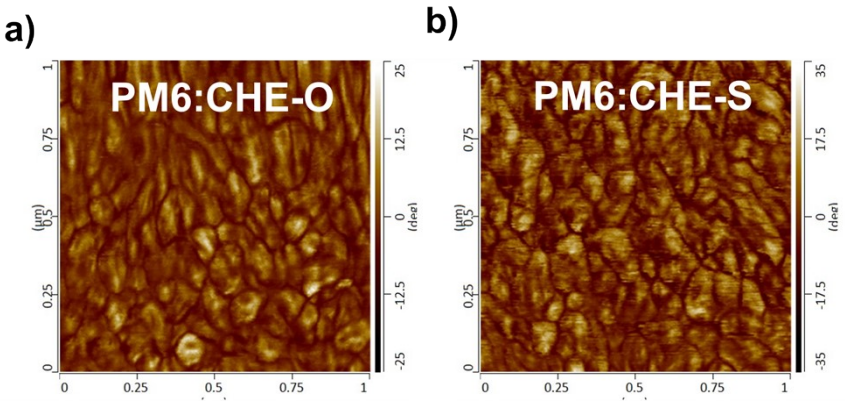

Figure S15: The AFM phase images of PM6: CHE-O and PM6: CHE-S.

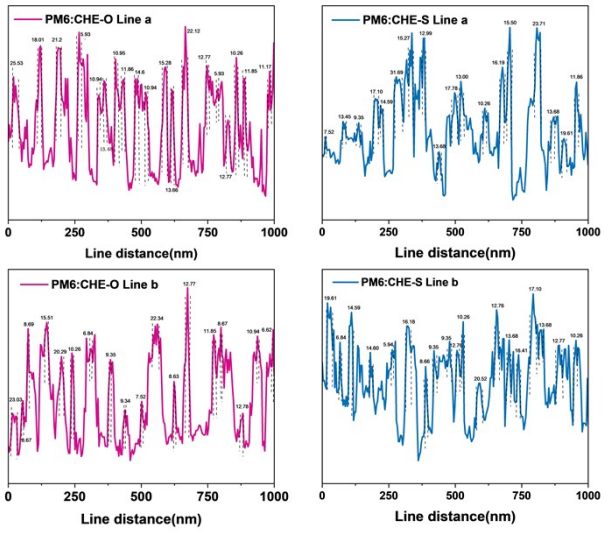

Figure S16. The line profile to obtain the fibril width form the AFM-IR images of PM6: CHE-O and PM6: CHE-S blended films.

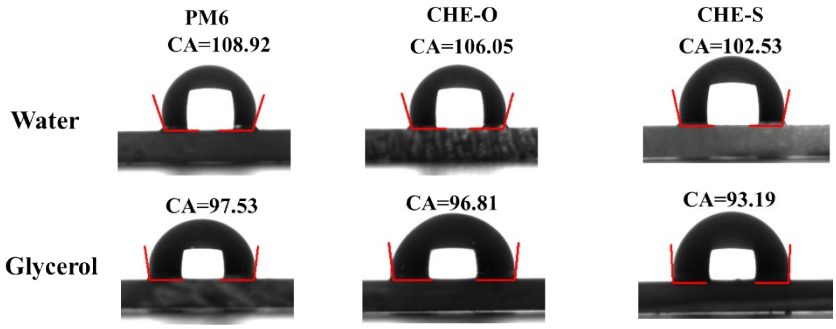

Figure S17. The images of water and glycerol drop on PM6, CHE-O and CHE-S neat films.

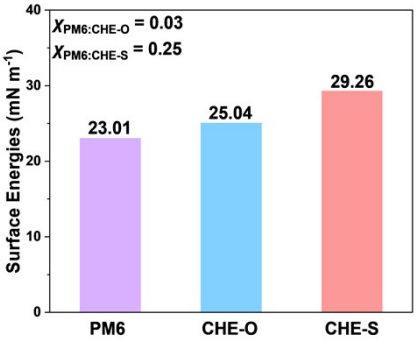

Figure S18. Summary of the surface energy of two SMAs and their Flory-Huggins interaction parameters with PM6.

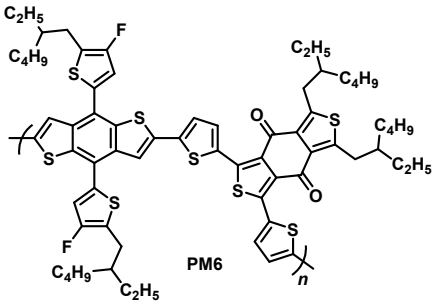

Figure S19: The chemical structure of PM6.

6. Spectral Charts of NMR and HR-MS

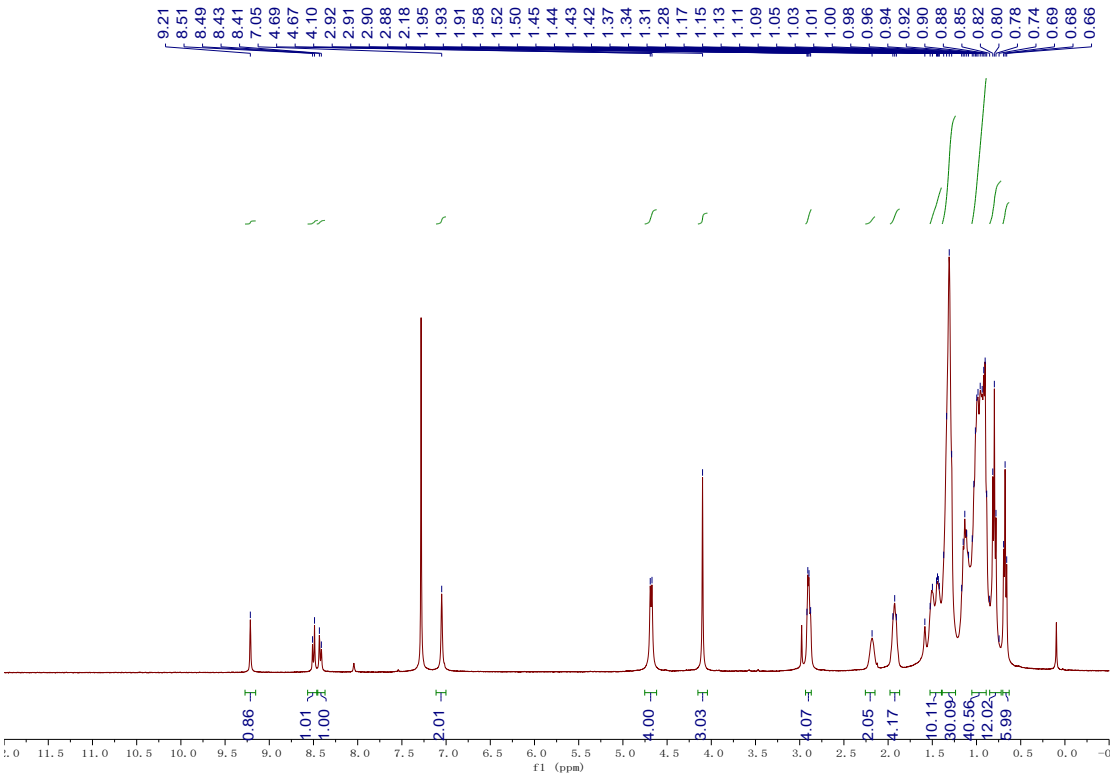

^{1}H NMR spectrum of **intermediate 2** in $CDCl_3$.

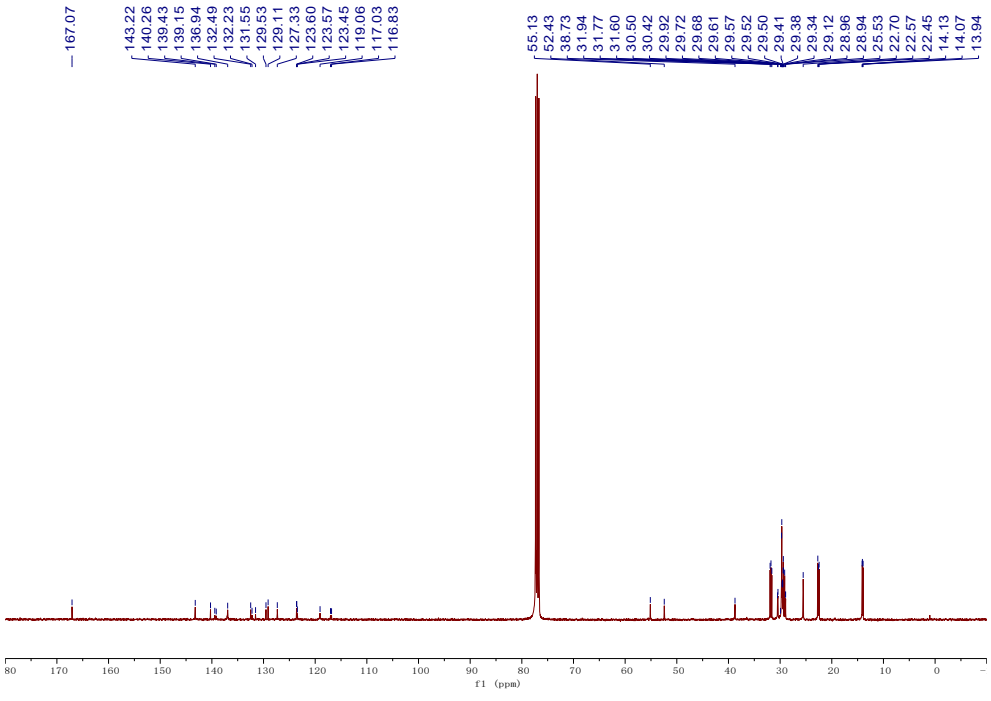

^{13}C NMR spectrum of **intermediate 2** in $CDCl_3$.

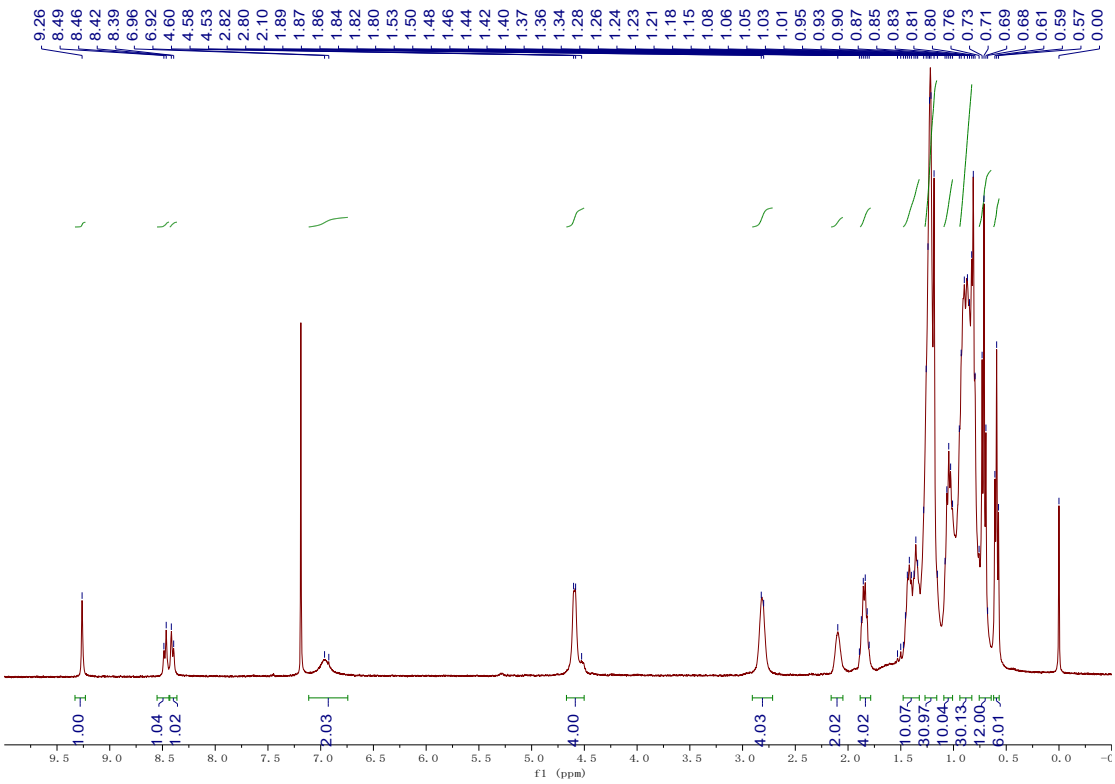

^{1}H NMR spectrum of **intermediate 3** in $CDCl_3$.

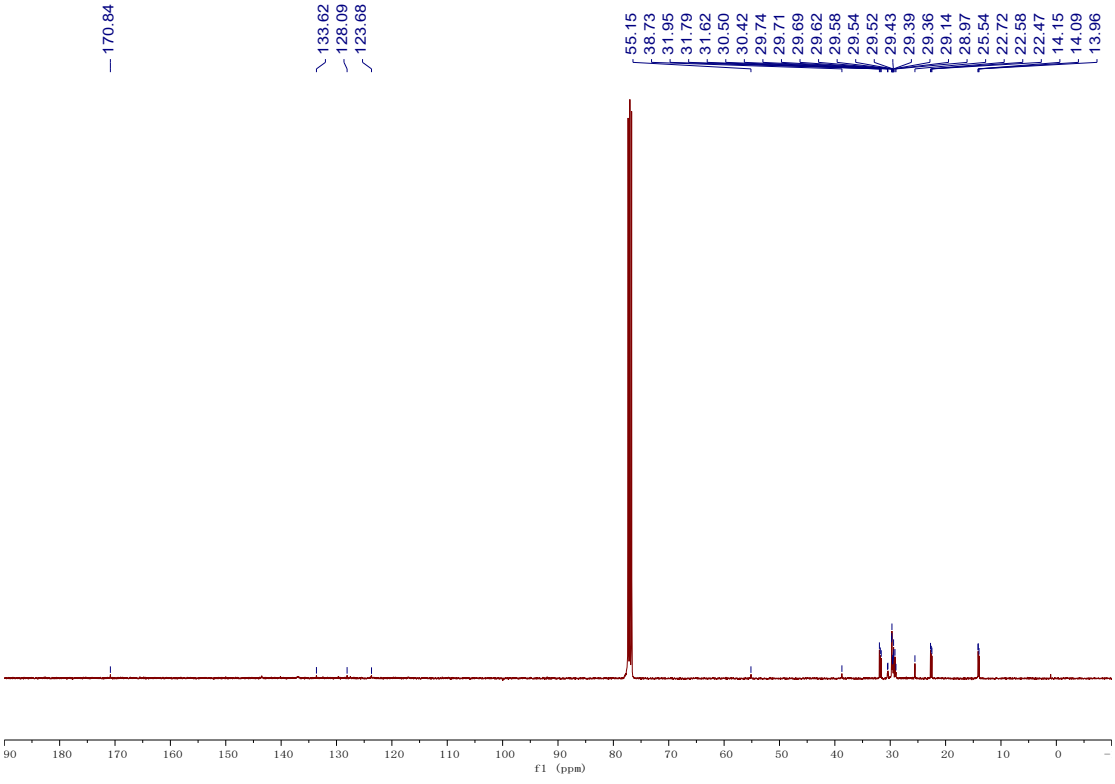

^{13}C NMR spectrum of **intermediate 3** in $CDCl_3$.

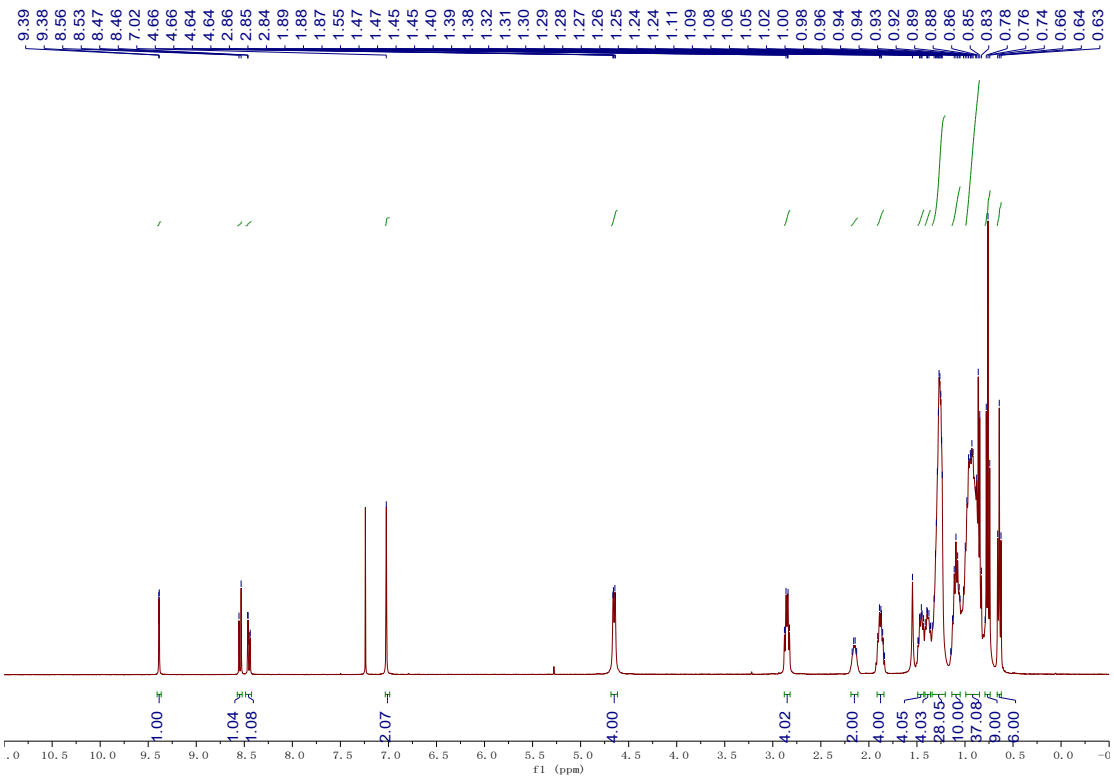

^{1}H NMR spectrum of **4a** in $CDCl_3$.

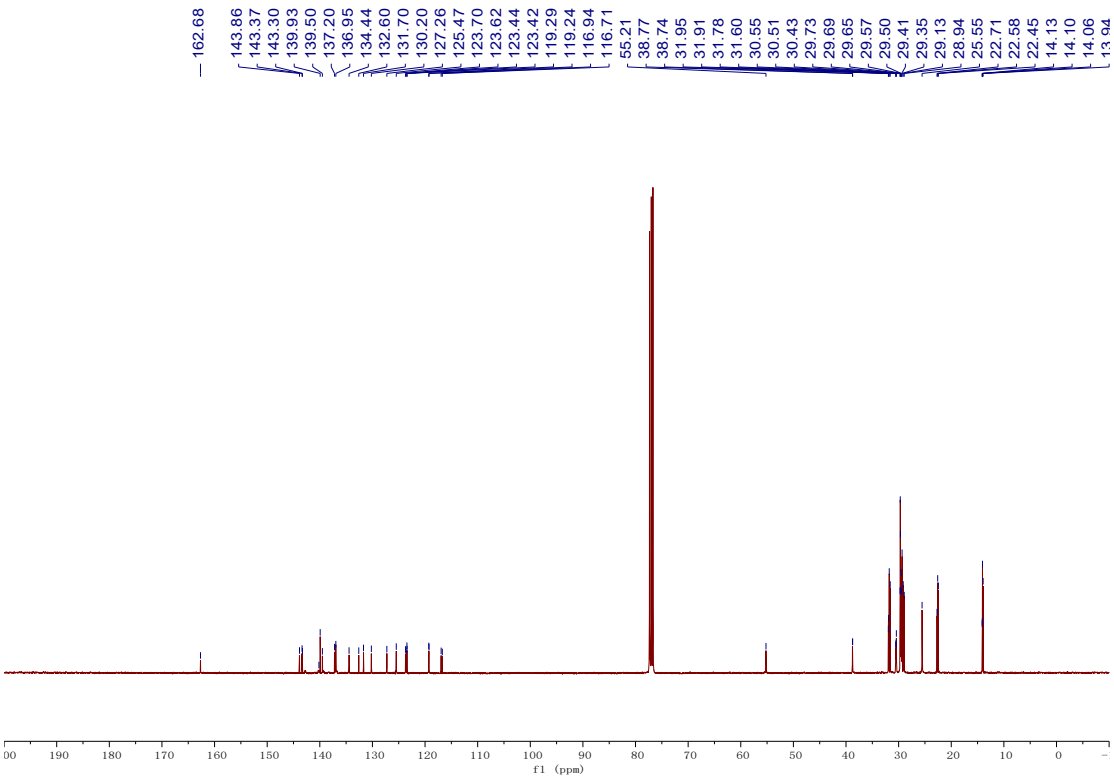

^{13}C NMR spectrum of **4a** in $CDCl_3$.

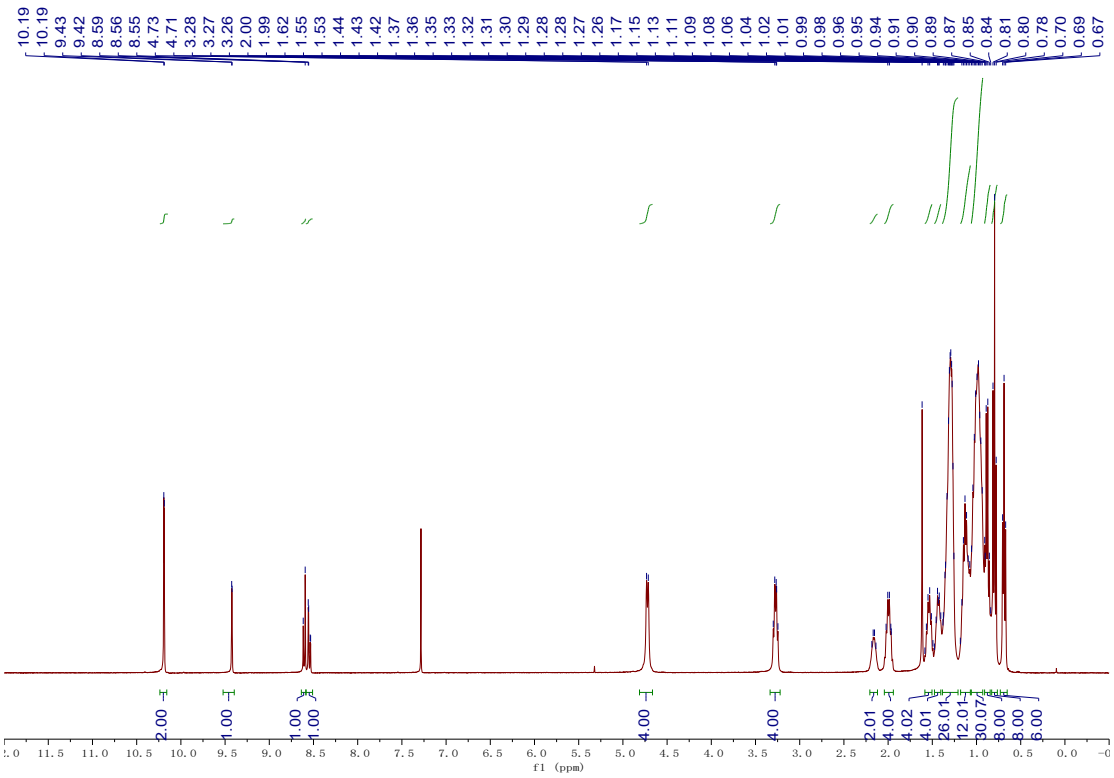

^{1}H NMR spectrum of **5a** in $CDCl_3$.

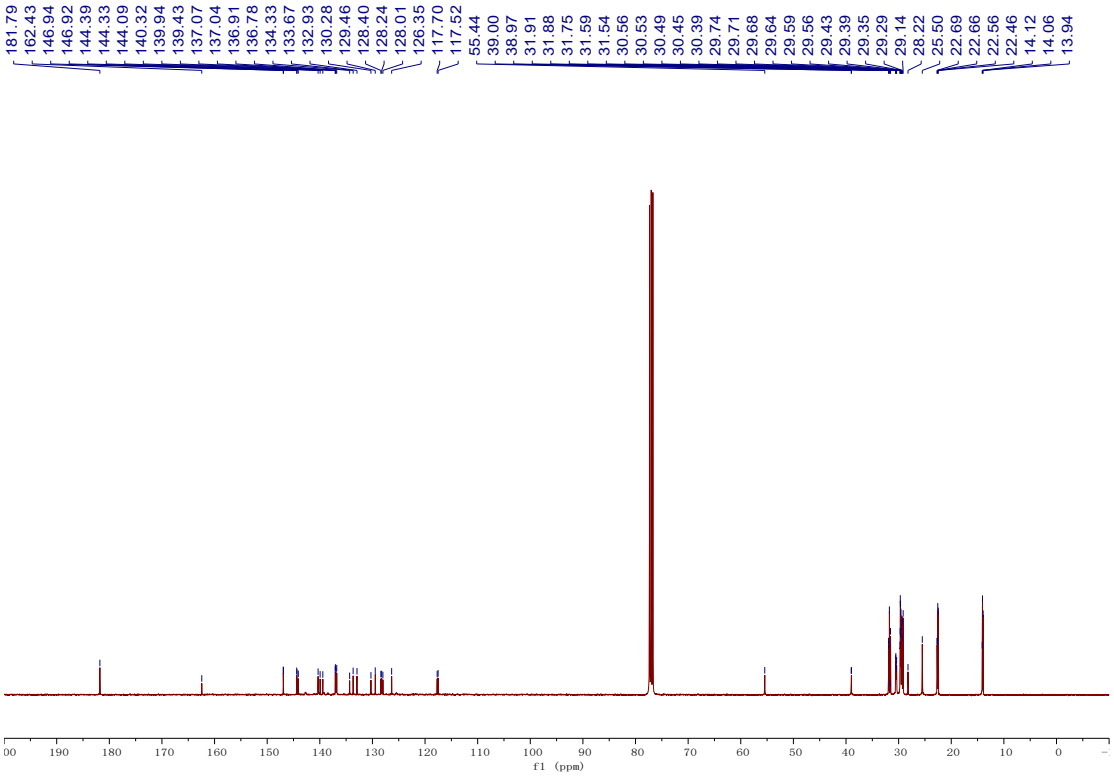

^{13}C NMR spectrum of **5a** in $CDCl_3$.

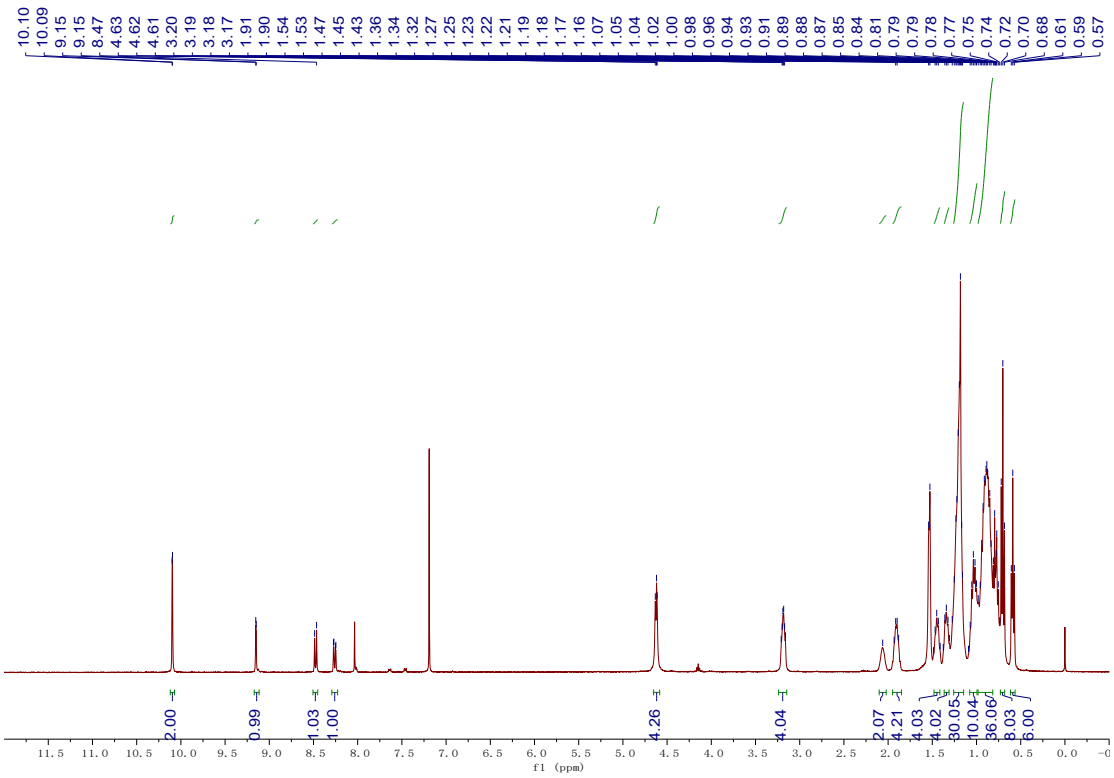

^{1}H NMR spectrum of **5b** in $CDCl_3$.

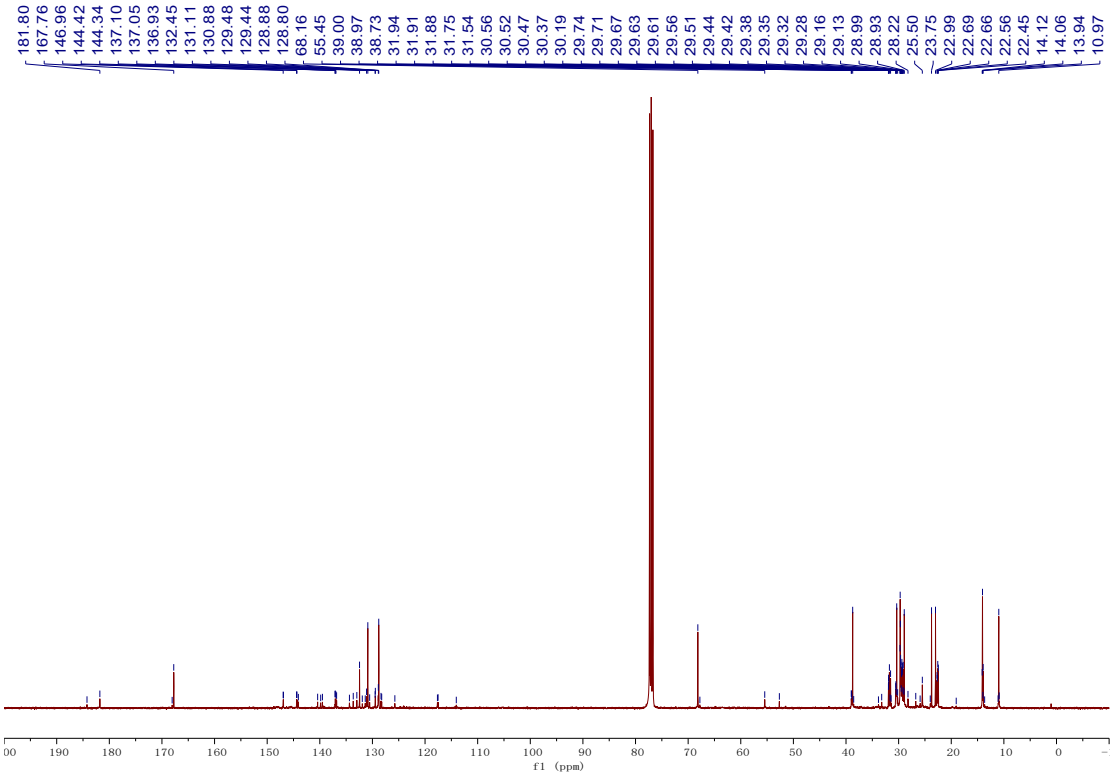

^{13}C NMR spectrum of **5b** in $CDCl_3$.

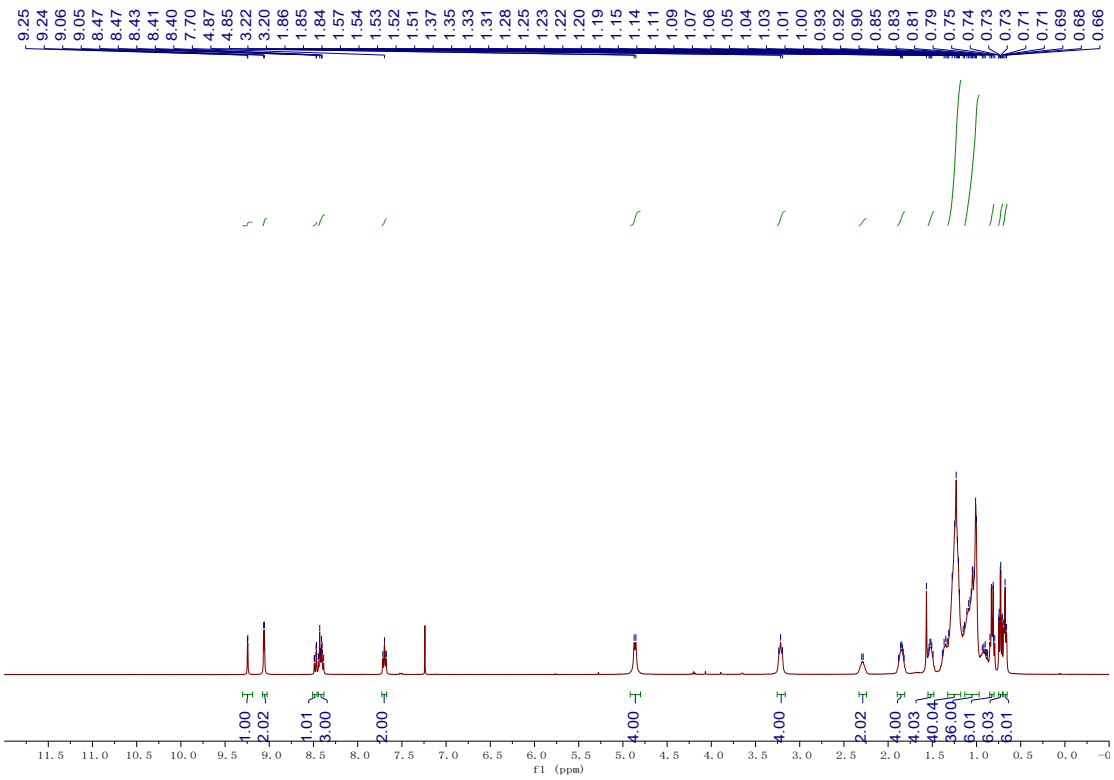

^{1}H NMR spectrum of **CHE-O** in $CDCl_3$.

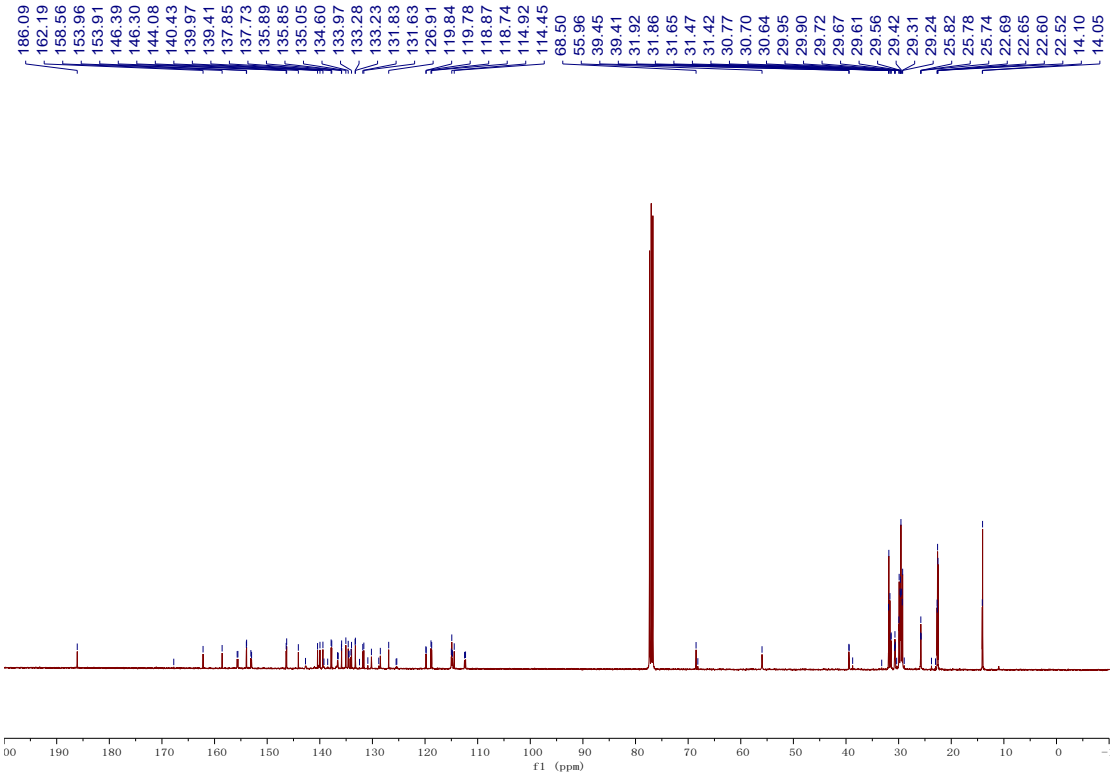

^{13}C NMR spectrum of **CHE-O** in $CDCl_3$.

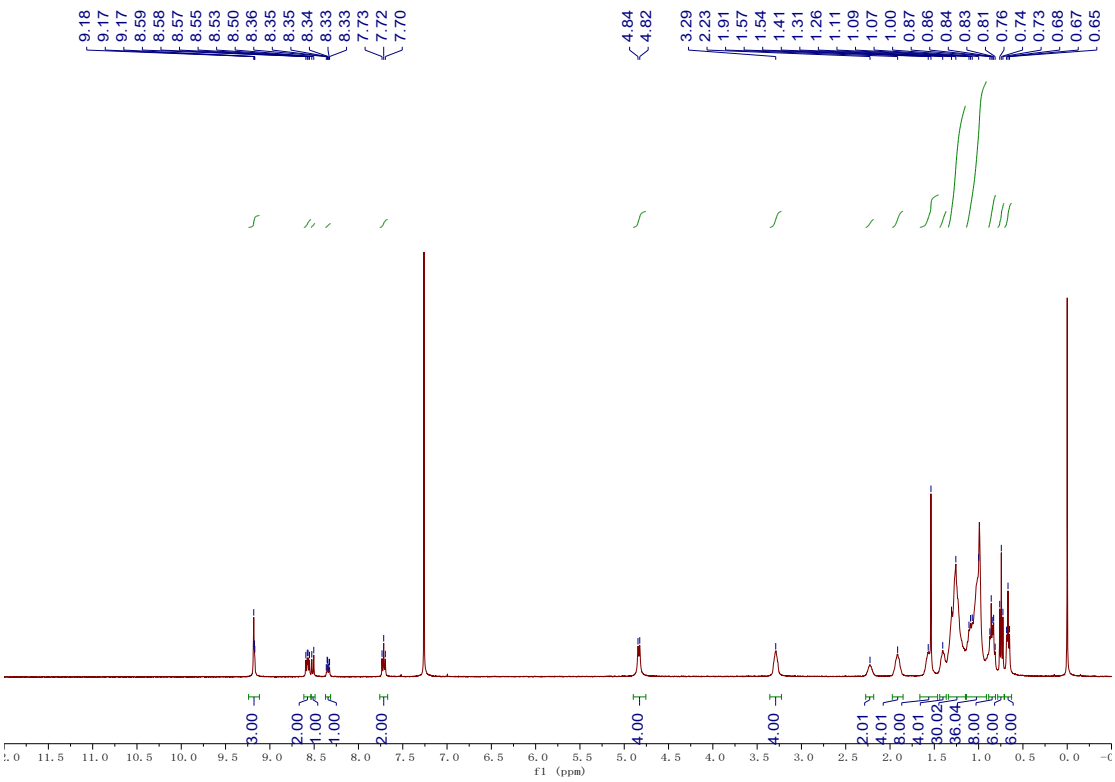

^{1}H NMR spectrum of **CHE-S** in $CDCl_3$.

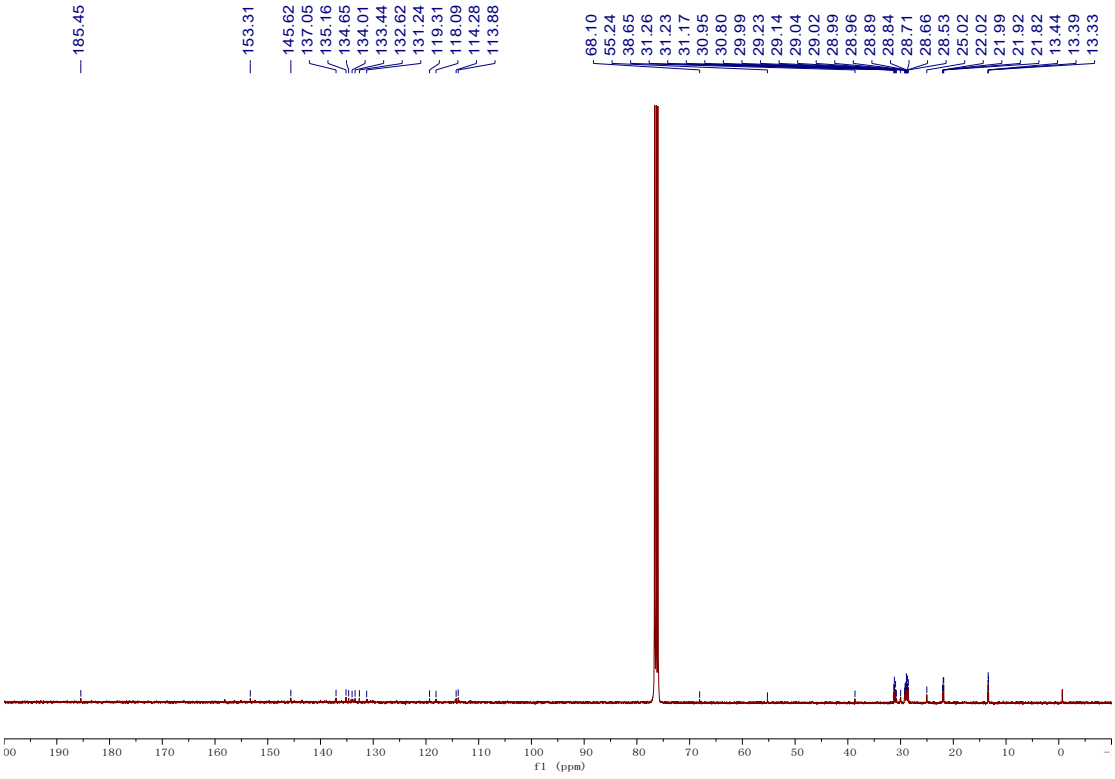

^{13}C NMR spectrum of **CHE-S** in $CDCl_3$.

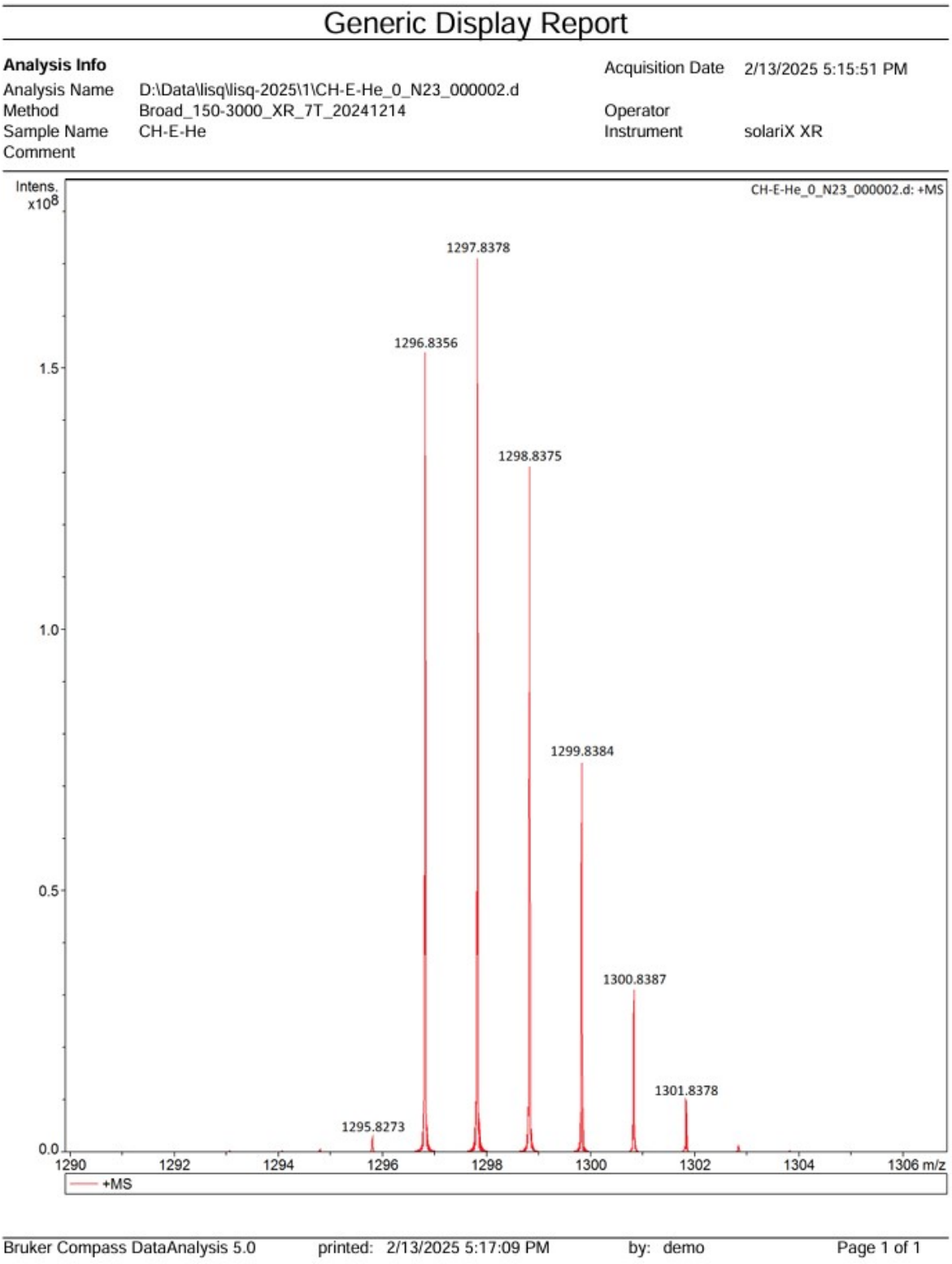

HRMS of **intermediate 2.**

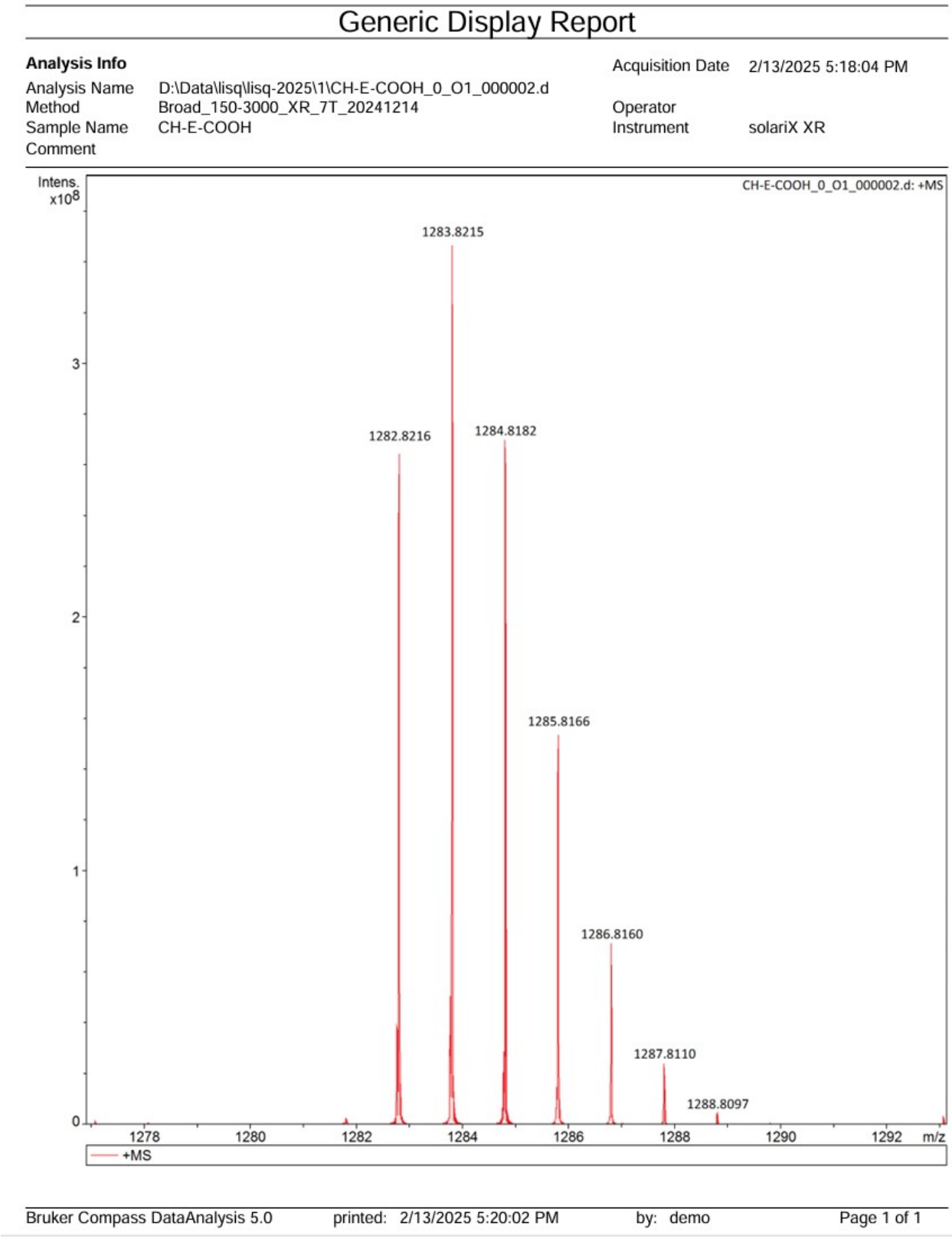

HRMS of **intermediate 3.**

Generic Display Report

Analysis Info

Analysis Name	D:\Data\lisq\lisq-2025\7\O-5F-He_0_E20_000001.d	Acquisition Date	7/8/2025 8:30:40 AM
Method	Broad_150-3000_XR_7T_20241214	Operator	
Sample Name	O-5F-He	Instrument	solariX XR
Comment			

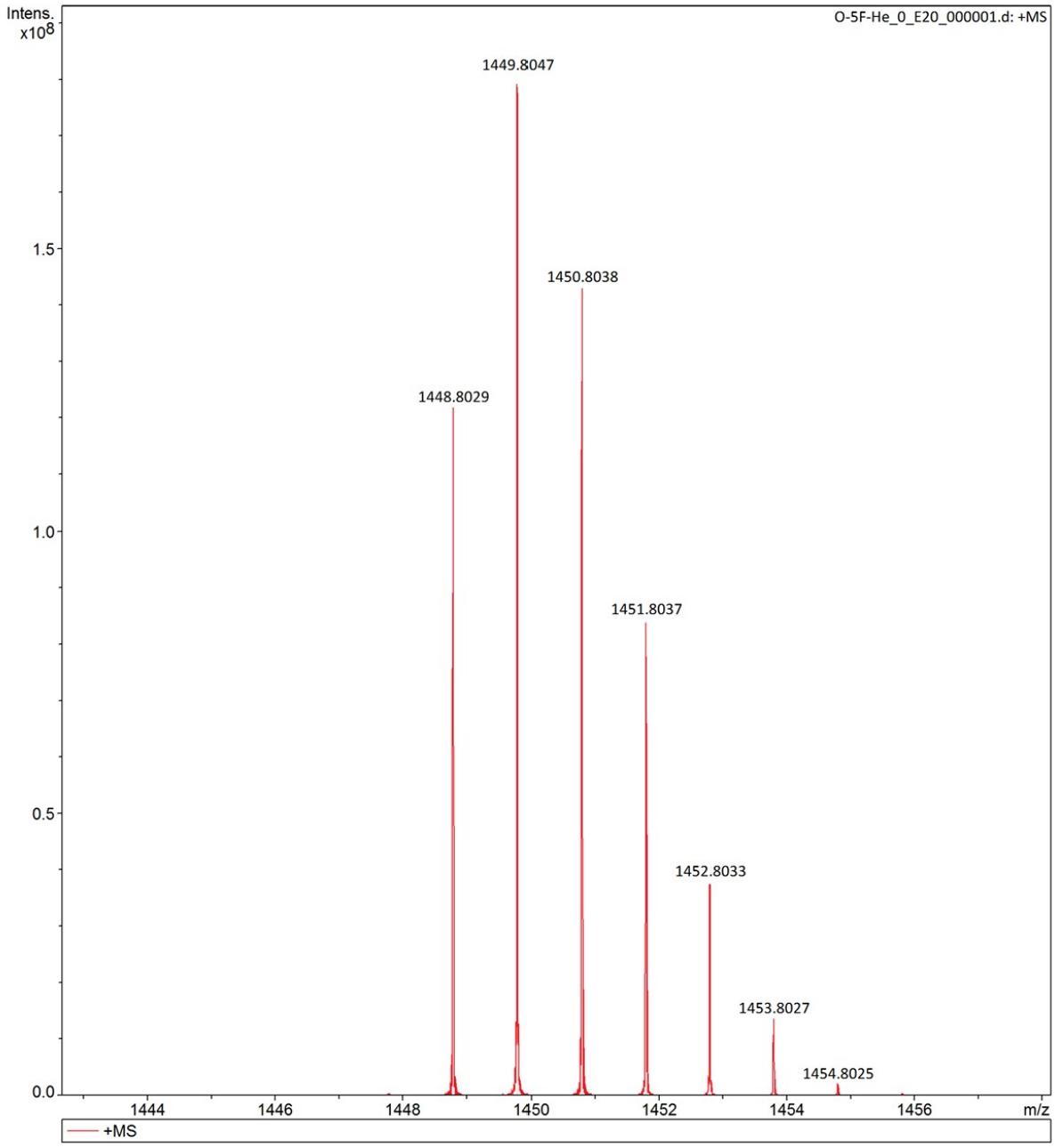

Bruker Compass DataAnalysis 5.0 printed: 7/8/2025 8:32:46 AM by: demo Page 1 of 1

HRMS of **intermediate 4a**.

Generic Display Report

Analysis Info

Analysis Name	D:\Data\lisq\lisq-2025\7\S-5F-He_0_E23_000001.d	Acquisition Date	7/8/2025 8:37:57 AM
Method	Broad_150-3000_XR_7T_20241214	Operator	
Sample Name	S-5F-He	Instrument	solariX XR
Comment			

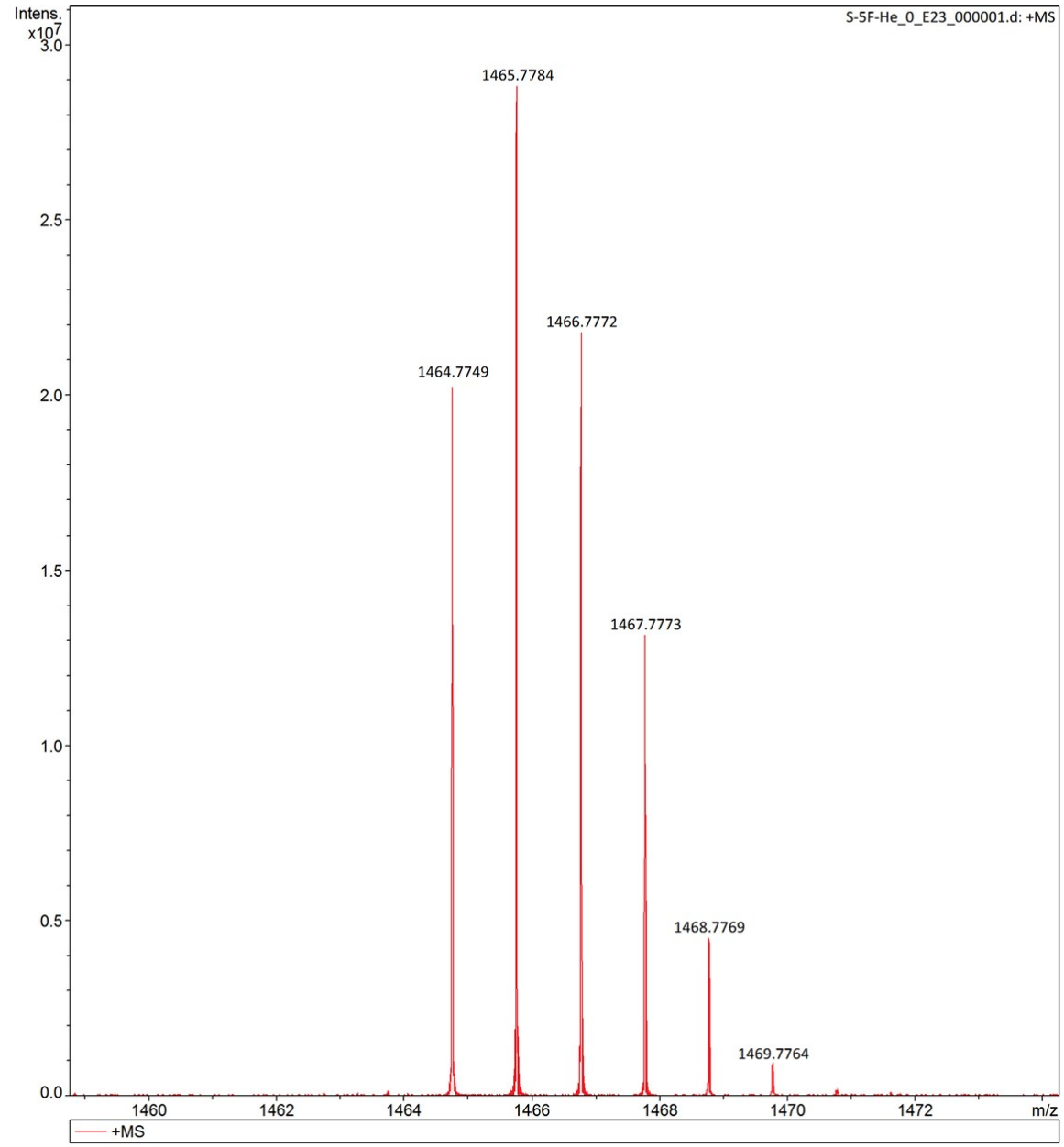

HRMS of **intermediate 4b**.

Generic Display Report

Analysis Info

Analysis Name	D:\Data\lisq\lisq-2025\7\O-5F-CHO_0_E21_000001.d	Acquisition Date	7/8/2025 8:33:24 AM
Method	Broad_150-3000_XR_7T_20241214	Operator	
Sample Name	O-5F-CHO	Instrument	solariX XR
Comment			

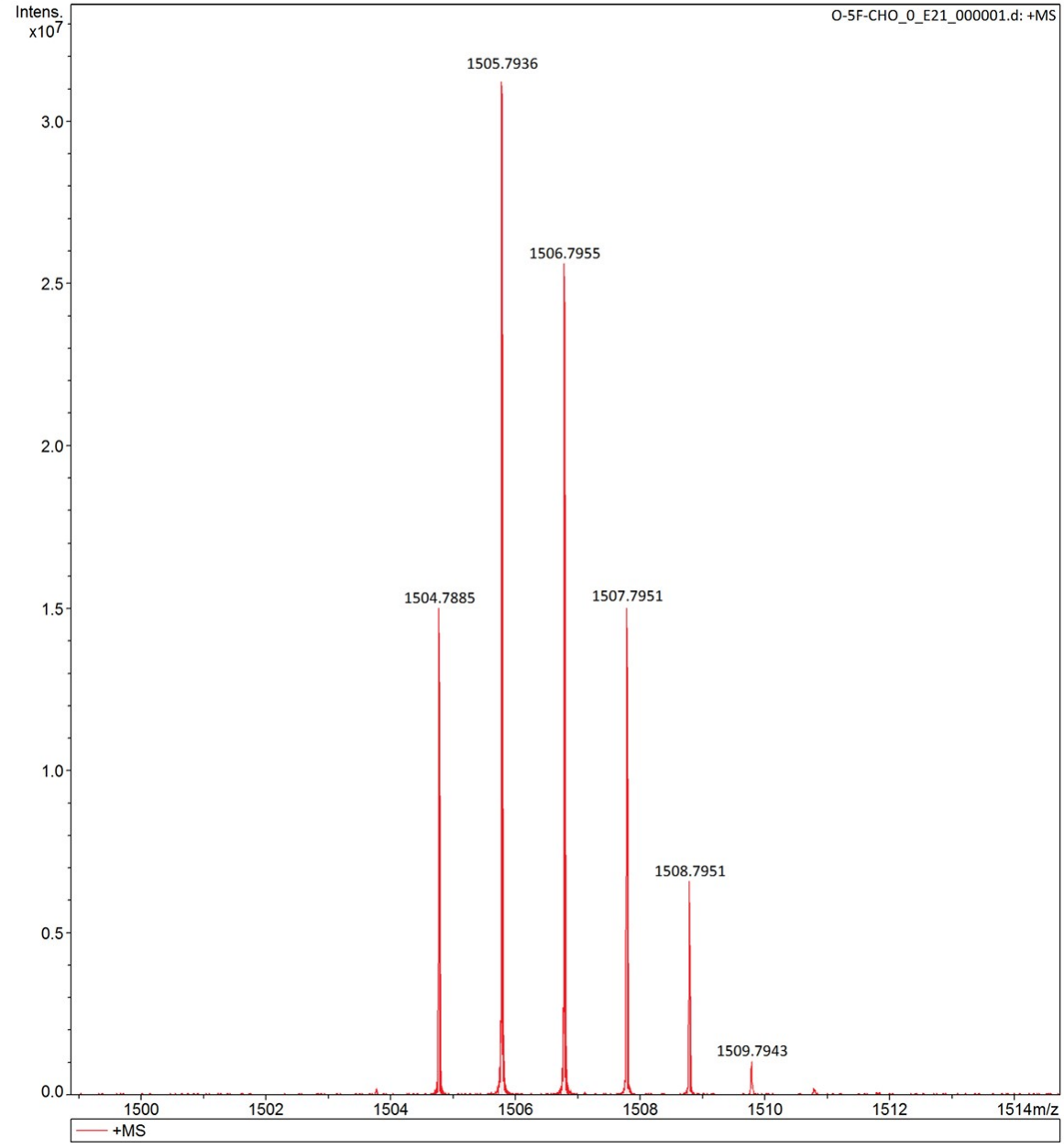

HRMS of **intermediate 5a**.

Generic Display Report

Analysis Info

Analysis Name	D:\Data\lisq\lisq-2025\7\O-5F_0_E22_000002.d	Acquisition Date	7/8/2025 8:36:17 AM
Method	Broad_150-3000_XR_7T_20241214	Operator	
Sample Name	O-5F	Instrument	solariX XR
Comment			

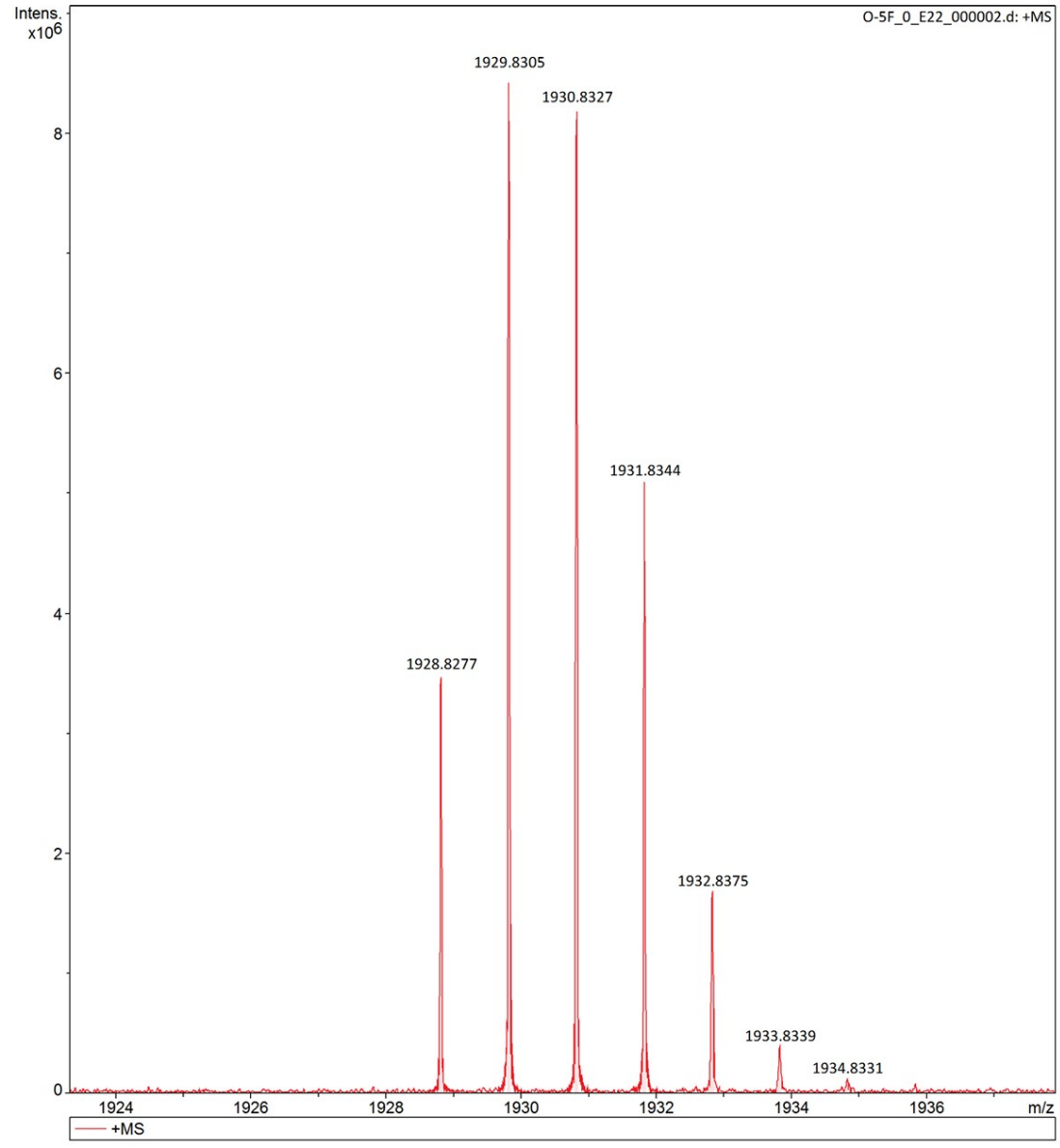

Bruker Compass DataAnalysis 5.0 printed: 7/8/2025 8:37:31 AM by: demo Page 1 of 1

HRMS of **CHE-O**.

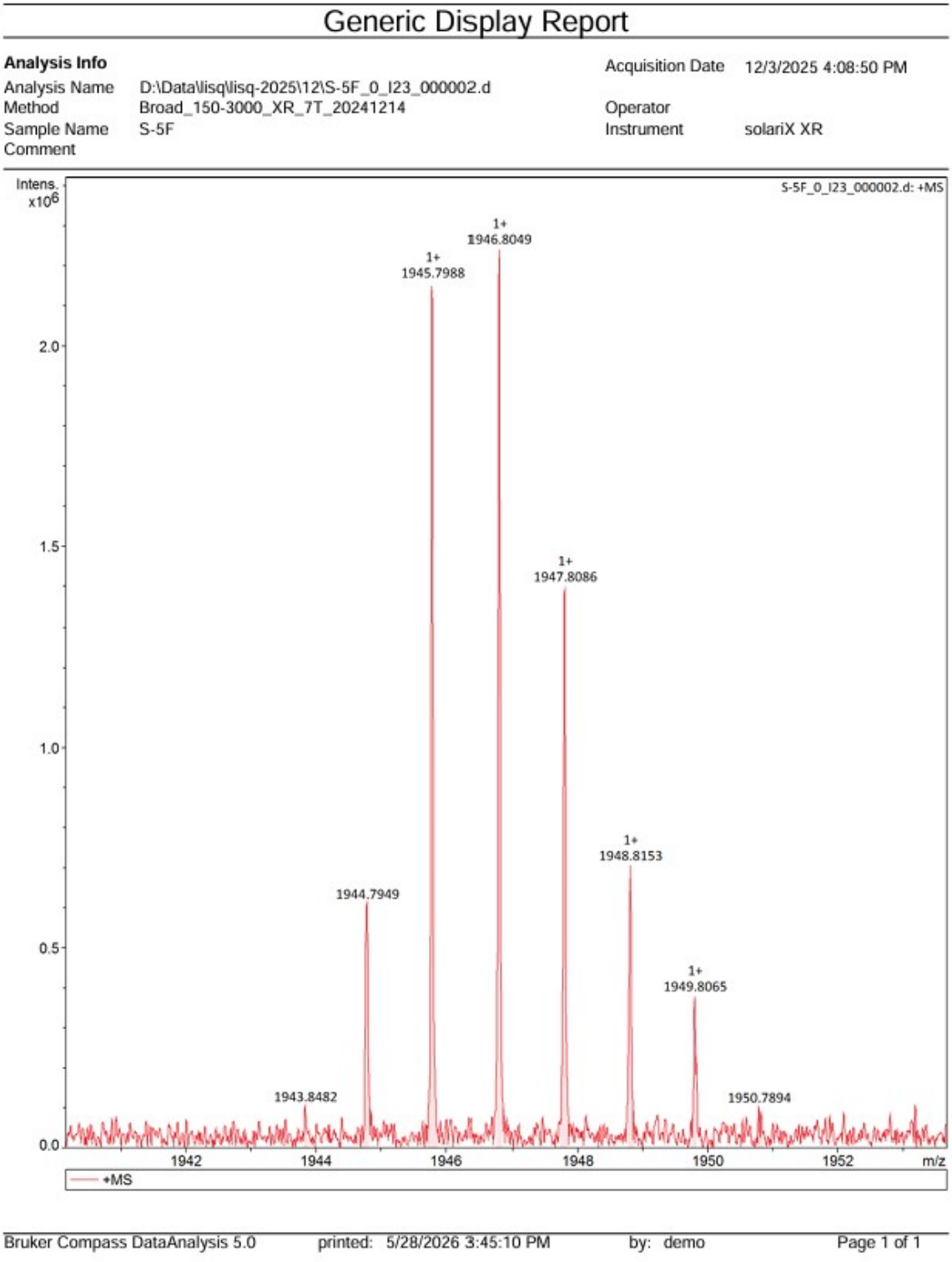
Generic Display Report
Analysis Info
Analysis Name D:\Data\lisq\lisq-2025\12\S-5F_0_I23_000002.d
Method Broad_150-3000_XR_7T_20241214
Sample Name S-5F
Comment
Acquisition Date 12/3/2025 4:08:50 PM
Operator
Instrument solariX XR
Intens. x10^6
S-5F_0_I23_000002.d: +MS
1+ 1946.8049
1+ 1945.7988
1+ 1947.8086
1+ 1948.8153
1+ 1949.8065
1944.7949
1943.8482
1950.7894
2.0
1.5
1.0
0.5
0.0
1942
1944
1946
1948
1950
1952
m/z
+MS
Bruker Compass DataAnalysis 5.0 printed: 5/28/2026 3:45:10 PM by: demo Page 1 of 1

HRMS of **CHE-S**.

7. Supplementary Reference.

[1] A. D. Becke, *J. Chem. Phys*. **1993**, 98, 5648-5652.

[2] P. C. Hariharan, J. A. Pople, *Mol. Phys*. **1974**, 27, 209-214.

[3] G. Frisch, J. Robb, M. C. Nakatsuji, M. Sonnenberg, J. B. F. Farkas, e. al., *Gaussian 16, Gaussian, Inc*.: Wallingford, CT **2016**.

[4] Dolomanov, O.V., Bourhis, L.J., Gildea, R.J, Howard, J.A.K. & Puschmann, H., *J. Appl. Cryst*. **2009**, 42, 339-341.

[5] Sheldrick, G.M. Acta Cryst. **2015**, A71, 3-8.